CrystEngComm

ROYAL SOCIETY OF CHEMISTRY

HIGHLIGHT

View Article Online
View Journal

Cite this: DOI: 10.1039/d5ce00772k

Hierarchical MOFs and derivatives toward advanced electrode materials for electrochemical energy storage

Zimeng Shao, Kai Shi, Jiahao Wei, Lina Zhou, * Dandan Han * and Junbo Gong

Received 2nd August 2025,
Accepted 9th September 2025

DOI: 10.1039/d5ce00772k

rsc.li/crystengcomm

Hierarchical metal–organic frameworks (MOFs) and their derivatives are categorized into three structural types: hierarchical porous structure, hierarchical architectural structure, and hierarchical compositional structure. With their structural diversity and ability to synergistically regulate electrochemical properties across multiple scales, hierarchical MOF materials have attracted widespread attention. This review systematically analyzes strategies for the three types of hierarchical MOFs and their derivatives, including the template guided method, additive-assisted modulation, etching, ion-exchange, self-assembly, and the *in situ* growth method. Recent applications of MOFs and their derivatives in electrochemical energy storage devices, including secondary batteries and supercapacitors, are also introduced. Finally, the structural advantages, challenges, and future research prospects of hierarchical MOFs and their derivatives are summarized.

1. Introduction

The utilization of green and sustainable energy sources has emerged as a pivotal approach to alleviating global reliance on fossil fuels and addressing environmental challenges. Among emerging technologies, electrochemical energy storage systems (EESS) stand out due to their flexibility, high energy storage capacity, and environmental benignity.[1] Although technologies such as solar and wind power have achieved significant advances in scalability and deployment, their inherent intermittency—due to diurnal and seasonal cycles and weather variability—poses critical challenges to grid stability.[2,3] To address this limitation, exploring advanced EESS with long-term cycling stability and reversible capacity has been deployed as an effective strategy. Consequently, significant research efforts are devoted to developing secondary batteries[4–14] and supercapacitors.[15,16] Crucially, the performance of these devices is intrinsically tied to the properties of their electrode materials, necessitating continuous innovation in material design.[17,18]

Metal–organic frameworks (MOFs), crystalline porous materials formed by coordinating inorganic metal ions with

State Key Laboratory of Chemical Engineering, School of Chemical Engineering and Technology, Tianjin University, Tianjin 300072, China.
E-mail: linazhou@tju.edu.cn, handandan@tju.edu.cn

Zimeng Shao

Zimeng Shao is currently a graduate student at the School of Chemical Engineering, Tianjin University, affiliated with the Gong group at the National Industrial Crystallization Center. Her research focuses on metal–organic framework materials and solid-state electrolytes for lithium-ion batteries.

Kai Shi

Kai Shi is a Master candidate at the School of Chemical Engineering, Tianjin University, affiliated with the Gong group at the National Industrial Crystallization Center. His research focuses on lithium-ion batteries, metal–organic framework materials, and two-dimensional materials for energy storage applications.

organic ligands,[19–21] have emerged as promising precursors for energy storage materials due to their exceptionally high surface area, tunable porosity, and structural adaptability.[22–28] Pristine MOFs with homogeneous structures suffer from intrinsic limitations, including poor electrical conductivity, low mechanical stability, and rapid capacity fading, which significantly hinder their practical deployment in high-energy-density electrochemical devices. To overcome these limitations, sophisticated design strategies for high-stability MOFs and derivatives have emerged. For instance, bimetallic MOFs like Zn–V frameworks exhibit enhanced electrical conductivity and operational stability, allowing their direct application as durable electrocatalysts.[29] Additionally, Liu *et al.* developed MOF-derived N,S-doped carbon nanorods coupled with iron phthalocyanines. Through the incorporation of carbon components and heteroatom doping, this hybrid structure exhibits enhanced mechanical strength and improved stability under harsh electrochemical conditions.[30] Notably, the incorporation of conductive materials, heteroatom doping, and morphological control serve as effective strategies to enhance the electrical conductivity, redox activity, and structural stability of MOFs.[31–35] More recently, the design of hierarchical structures—inspired by natural systems like bone and nacre—has emerged as a powerful strategy to synergistically integrate the advantages of various approaches. Hierarchical MOFs and their derivatives simultaneously optimize ion transport pathways, enhance structural stability, and maximize active site exposure, thereby amplifying the performance of MOF-based materials.[36] The concept of hierarchical materials, defined by Lakes in 1993, describes systems with multiple distinct structural levels in which substructures interact to optimize overall properties and functionality.[37] Building upon this foundation, Zhou *et al.* adapted and applied the concept of hierarchical materials specifically to MOFs in 2020.[38] They categorized hierarchical MOFs into three primary types based on their defining characteristics: hierarchical porous structure, hierarchical architectural structure, and hierarchical compositional structure (Fig. 1). (1) Hierarchical porous MOF-based systems integrate intrinsic micropores, mesopores, and macropores to enable multifunctional energy storage.[39] (2) Hierarchical architectural structure morphological designs include core–shell, hollow, and yolk–shell configurations. (3) Hierarchical compositional structures result from incorporating distinct chemical components or phases within a material to achieve

Jiahao Wei

Jiahao Wei is a PhD student at the School of Chemical Engineering, Tianjin University. His research interests focus on functional crystal materials and catalytic processes.

Lina Zhou

Lina Zhou is an Associate Researcher at the School of Chemical Engineering and Technology, Tianjin University. She currently conducts research at the National Engineering Research Center of Industrial Crystallization Technology, focusing on polymorph analysis, pilot-scale crystallization, chiral resolution, and crystal engineering.

Dandan Han

Dandan Han is an Associate Researcher at Tianjin University. She currently conducts research at the National Engineering Research Center of Industrial Crystallization Technology, focusing on crystal growth mechanisms, crystal habit control, chiral separation, and the design of multicomponent pharmaceutical crystals.

Junbo Gong

Junbo Gong is a Professor at Tianjin University, the Deputy Director of the National Engineering Research Center of Industrial Crystallization Technology, and the Executive Director of the National Research Center for Crystallization Science and Engineering. His current research mainly focuses on crystal engineering and functional crystalline materials.

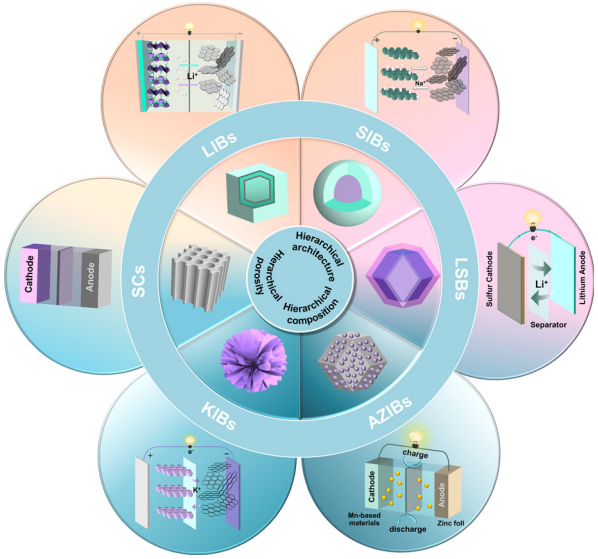

Fig. 1 The structures and applications of hierarchical MOFs and their derivative materials.

heterogeneous functionality. Thus, the strategic design of MOFs and their derivatives incorporating these hierarchical structural features presents a highly promising avenue for next-generation EESS.

The past decade has witnessed substantial progress in designing hierarchical electrode materials with tailored porosity, architecture, and composition, driven by the pursuit of enhanced electrochemical performance (Fig. 2). Early breakthroughs, such as the pioneering work on multi-shelled Fe_2O_3 microboxes by Lou's group, demonstrated the profound impact of architectural design on electrochemical performance, particularly in mitigating volume expansion for metal oxide anodes.[40,41] These seminal studies stimulated broad interest in utilizing diverse hollow and core–shell MOF-derived architectures as a strategic solution to critical challenges like volume expansion and capacity degradation.[42–44] Parallel efforts focused on constructing hierarchical heterostructures, integrating conductive matrices such as carbon nanotubes and graphene with active materials to synergistically enhance electrical conductivity and mechanical stability.[45–48] Furthermore, the engineering of hierarchical porosity—incorporating macropores and mesopores alongside micropores—has proven effective in shortening ion diffusion paths and enhancing ion transport, thereby boosting rate capability and cycling stability.[49–51]

As research progressed, the challenge shifted from merely creating hierarchical structures to precisely synthesizing them with intricate control, marking a new frontier in the field. This pursuit of precision has led to the creation of

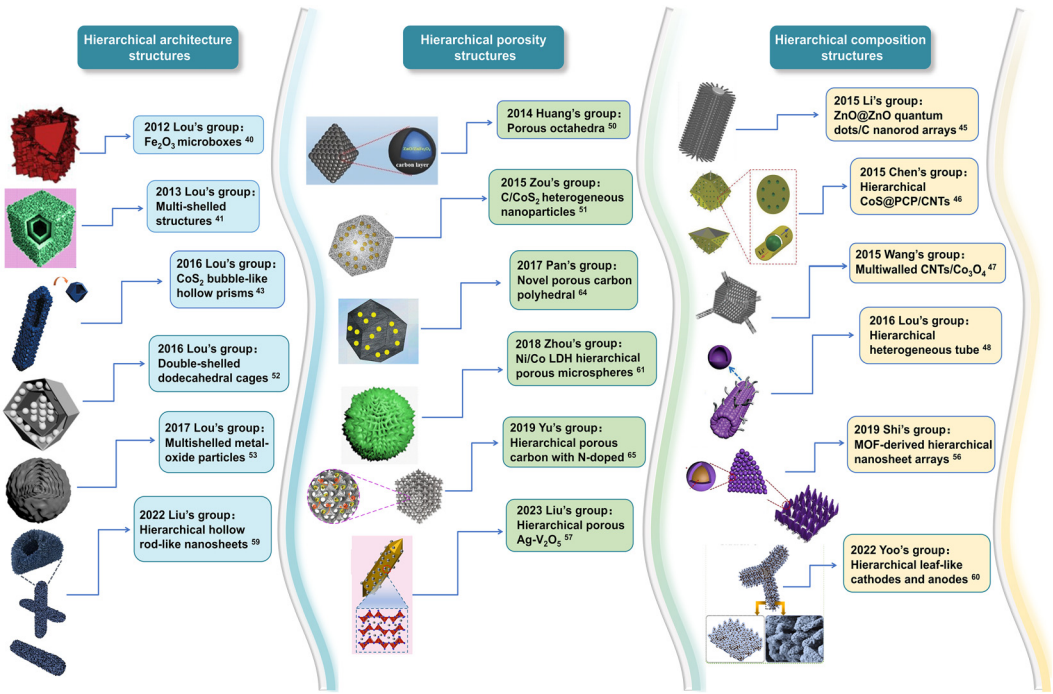

Fig. 2 A development process of hierarchical MOFs and their derivatives. Reproduced with permission from ref. 40, copyright 2012, American Chemical Society; reproduced with permission from ref. 41, copyright 2013, American Chemical Society; reproduced with permission from ref. 43, copyright 2016, WILEY-VCH; reproduced with permission from ref. 45, copyright 2015, WILEY-VCH; reproduced with permission from ref. 46, copyright 2015, WILEY-VCH; reproduced with permission from ref. 47, copyright 2015, American Chemical Society; reproduced with permission from ref. 48, copyright 2016, WILEY-VCH; reproduced with permission from ref. 50, copyright 2014, WILEY-VCH; reproduced with permission from ref. 51, copyright 2015, WILEY-VCH; reproduced with permission from ref. 52, copyright 2016, WILEY-VCH; reproduced with permission from ref. 53, copyright 2017, WILEY-VCH; reproduced with permission from ref. 56, copyright 2019, Elsevier; reproduced with permission from ref. 57, copyright 2023, Elsevier; reproduced with permission from ref. 59, copyright 2021, Elsevier; reproduced with permission from ref. 60, copyright 2022, Elsevier; reproduced with permission from ref. 61, copyright 2019, American Chemical Society; reproduced with permission from ref. 64, copyright 2017, Elsevier; reproduced with permission from ref. 65, copyright 2019, American Chemical Society.

increasingly sophisticated nanostructures with meticulously controlled geometries,[52–55] composition,[56] and porosity.[57] The research focus has expanded to leverage the inherent advantages of polymetallic oxides and sulfides and to combine multiple hierarchical features,[58–66] aiming to create materials with abundant electroactive sites, shortened ion/electron pathways, and enhanced synergistic effects. Collectively, these advancements underscore a paradigm shift from simple material synthesis to the precise fabrication of complex hierarchical architectures, paving the way for next-generation energy storage devices.

In light of these rapid advancements, this review systematically summarizes the latest developments in hierarchical MOFs and their derivatives for electrochemical energy storage. First, we elucidate the dominant synthesis strategies for creating hierarchical structures. Subsequently, we critically evaluate their applications across major energy storage devices, including secondary batteries and supercapacitors, discussing the structure–performance relationships. Finally, we discuss the scientific significance of hierarchical material design, current technological challenges, and future research directions to advance next-generation energy storage systems.

2. Synthesis method

Based on the classification of hierarchical MOFs and their derivative materials, we divide the synthesis methods into the following three categories: i) the synthesis methods of hierarchical architectural structures; ii) the synthesis methods of hierarchical compositional structures; iii) the synthesis methods of hierarchical porous structures. This section emphasizes categorizing the synthesis methods and presenting them in detail with updated or typical examples. The advantages, limitations, key parameters, and applications of different synthesis methods are summarized in Table 1.

2.1 Synthesis strategies of hierarchical architectural structures

2.1.1 Template guided method. As the primary synthesis strategy examined herein, the template-guided approach is systematically classified into three distinct categories based on template characteristics: hard-templates, soft-templates, and self-templates. The methodology fundamentally relies on two stages: template formation followed by its selective removal. Consequently, judicious selection of template types and precise optimization of removal parameters critically govern the successful fabrication of hierarchically structured MOF architectures.[67]

2.1.1.1 Hard template method. The hard-template method offers exceptional versatility in fabricating hollow MOF architectures, where pre-formed sacrificial templates dictate the final morphology with high precision. This methodology involves three sequential steps: (i) fabrication of dimensionally controlled templates, (ii) conformal MOF growth on template surfaces, and (iii) selective template removal *via* thermal decomposition or chemical etching.

Commonly used templates, such as polystyrene (PS) spheres, silica nanoparticles, and metal oxides, provide rigid spatial confinement, ensuring structural regularity and facilitating the construction of complex architectures. Consequently, this technique enables precise regulation of cavity dimensions and shell thickness, facilitating the engineering of hierarchical MOF structures with tailored porosity.[68,69] Li *et al.* devised a novel dual template strategy to construct MOF-derived $NiCo_2S_4$/MXene/N-doped carbon hollow microspheres.[70] This architecture is particularly innovative for overcoming the intrinsic low conductivity of MOFs by integrating highly conductive MXene nanosheets and carbon frameworks, resulting in exceptional performance in hybrid supercapacitors. In their synthesis, MXene was first anchored onto PS microspheres, utilizing its strong affinity for Co^{2+} ions to direct the subsequent *in situ* growth of ZIF-67. Subsequent ion exchange and thermal

Table 1 Summary of synthesis methods

Method	Dominance	Limitation	Parameters	Example	Reference
Hard template	Precise structural control	Requires template removal	Template size, removal methods	$NiCo_2S_4$/MXene/NC	70
				N-HPC	65
Soft template	Mild synthesis conditions	Inhomogeneous structure, instability	Template type, concentration, metal/ligand ratio	ZIF-8 hollow nanospheres	76
				Zr-MOF	77
Self-template	Eliminates template removal	Requires precursor design	High energy consumption, limits mass production	Co_3O_4@$Co_3V_2O_8$	78
				CoO/Co–Cu–S HTHSs	79
Additive-assisted modulation	Controlled crystal morphology	Requires additive removal	Additive type and concentration, reaction time	Mn-TH5	80
				MnHCF@Fe/MnHCF	81
Etching	High-precision structure regulation	Accurate control of conditions	Etchant type and concentration, reaction time	H-Co_3O_4@MCNBs	82
				Ni–NC(p)	83
Ion exchange	Efficient and eco-friendly	Ion diffusion rate affects reaction progress	Ion concentration	Cu–$CoSe_2$	84
Self-assembly	Facile processing	Poor stability	Reaction parameters	CN-TC@FG	85
In situ growth	Accurate structural tailoring	Multiple reaction steps, high energy consumption	Structural design of the precursor	Cu_3P/Cu@CNHO	86

sulfidation then converted the ZIF-67 into a stable bimetallic sulfide while simultaneously removing the template, yielding a hierarchical hollow structure (Fig. 3a). This synergistic integration of 2D MXene with MOFs represents a groundbreaking strategy to mitigate the poor electrical conductivity of MOFs, thereby unlocking their full potential in electrochemical applications.[71–73] Besides polymeric templates, inorganic alternatives such as silica nanoparticles offer versatile platforms for hollow structure synthesis. For instance, Azhar *et al.* utilized spherical silica templates for CoFe–Prussian blue analogue (PBA) nucleation, followed by HF etching to yield hollow MOF electrodes.[74]

The hard-template method is highly capable of fabricating sophisticated architectures, including hollow and core–shell structures, with remarkable accuracy. Its generality across a wide range of MOFs and their derivatives is one of its greatest strengths, enabling the synthesis of diverse functional materials. However, a significant challenge lies in the template removal step, which frequently requires harsh conditions such as high temperatures or corrosive etchants. These conditions can compromise the stability of the frameworks, potentially leading to structural collapse, pore blockage, or the introduction of defects.

2.1.1.2 Soft template method. The soft-template approach typically involves three key steps: surfactant self-assembly into micelles, directed MOF crystallization, and template elimination, all under mild synthetic conditions.[75] In contrast to hard-templating that often employs corrosive etchants risking structural damage and environmental harm, the soft-templating route utilizes surfactant or emulsion templates to orchestrate hierarchical structures under benign conditions, thereby preserving framework integrity.

The soft-template synthesis of MOFs and their derivatives with hollow architectures commonly employs emulsion-assisted strategies as a versatile design platform. A notable innovation was demonstrated by Pang *et al.*, who first

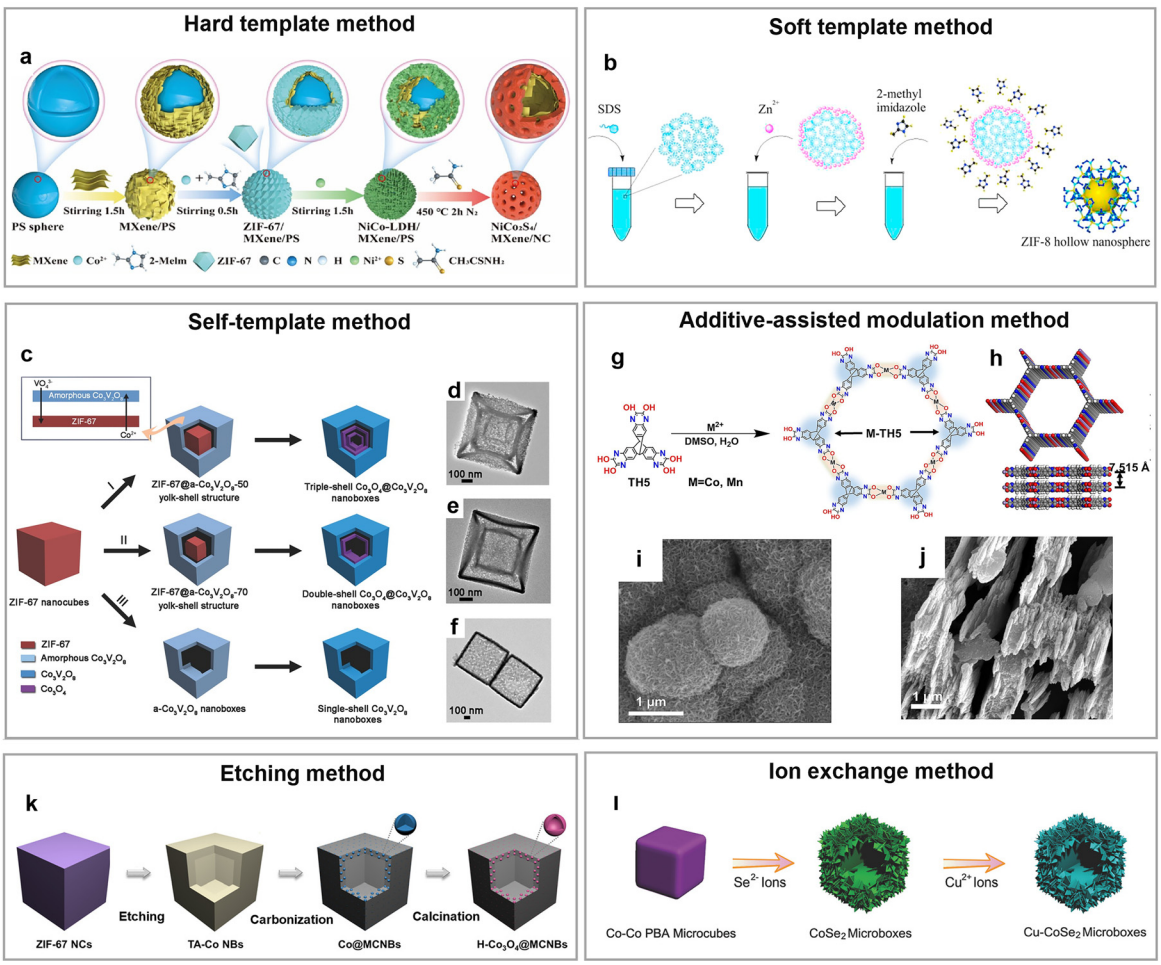

Fig. 3 Some typical synthesis strategies of hierarchical architectural structures: (a) schematic diagram of $NiCo_2S_4$/MXene/NC; reproduced with permission from ref. 70. Copyright 2024, Elsevier. (b) Schematic diagram of ZIF-8 hollow nanospheres; reproduced with permission from ref. 76. Copyright 2015, Elsevier. (c) Schematic diagram of Co_3O_4@$Co_3V_2O_8$ hollow structures; (d–f) TEM images of the corresponding products; reproduced with permission from ref. 78. Copyright 2017, WILEY-VCH. (g) Synthetic diagram of M-TH5; (h) 3D view of M-TH5; (i) SEM image of Mn-TH5; (j) SEM image of Co-TH5; reproduced with permission from ref. 80. Copyright 2024, Elsevier. (k) Schematic diagram of the formation process of H-Co_3O_4@MCNBs; reproduced with permission from ref. 82. Copyright 2020, Wiley-VCH. (l) Schematic illustration of the synthesis of Cu–$CoSe_2$ microboxes; reproduced with permission from ref. 84. Copyright 2018, Wiley-VCH.

described a one-step emulsion technique to assemble 3D hollow colloidosomes from faceted Fe-soc-MOF cubic building blocks—a significant departure from traditional spherical particle-based colloidosomes.[87] In this process, Tween-85 stabilized uniform emulsion droplets, which upon heating guided the oriented attachment of MOF cubes into monolayer shells, ultimately forming hollow architectures upon solvent evaporation. Besides emulsions, molecular surfactants alone can also serve as effective soft templates. Cao *et al.* synthesized ZIF-8 hollow nanospheres *via* a sodium dodecyl sulfate (SDS)-assisted soft-template strategy.[76] Above the critical micelle concentration (CMC), SDS self-assembles into micelles, enabling Zn^{2+} adsorption at hydrophilic interfaces for ligand coordination (Fig. 3b). Subsequent centrifugation and drying yield monodisperse hollow nanostructures. Pushing the boundaries of architectural control, Li *et al.* devised an innovative dual-surfactant (P123/F127) nanoemulsion system that enabled the precise synthesis of Zr-MOFs with a diverse array of architectures—from dendritic nanospheres to crumpled nanosheets—tailored for bulky molecules.[77] Additionally, Du *et al.* first demonstrated metal–sodium deoxycholate hydrogel as a soft template to fabricate hollow nanotube and nanosphere MOF structures.[88] The above research studies demonstrate the diversity of soft template selection.

Collectively, modulating the concentration and dosage of surfactants or emulsifiers permits precise morphological control in soft-template synthesis. Significantly, the expanding diversity of soft templates offers versatile platforms for designing hierarchical MOF-based architectures. Moreover, the soft template method enables morphology modulation of hierarchical structures under mild conditions by leveraging the coordination chemistry of MOFs. Despite these advancements, challenges remain for the electrochemical application of soft-templated MOFs, particularly regarding scalability, cost-effectiveness, and structural uniformity. The removal of soft templates under mild conditions often risks incomplete elimination, potentially blocking pores and reducing active site accessibility. Furthermore, achieving reproducible synthesis with precise structural control and ensuring long-term stability during electrochemical cycling are critical hurdles that must be overcome to transition these innovative materials from laboratory-scale research to practical applications. Crucially, facilitating the use of soft-templating for synthesizing MOF-derived hierarchical structures such as nanospheres and nanosheets will extend the application scope of this strategy from biosensing and enzyme immobilization to energy storage and catalysis.

2.1.1.3 Self-template method. Driven by the limitations of conventional templating methods—specifically, the requirement for high-temperature and toxic chemical etching in hard-templating removal and the high costs and limited structural stability of soft-templating—the self-template strategy has emerged as a prominent alternative for fabricating hierarchical hollow structures.[89] This approach entails synthesizing MOF-based precursors, which are subsequently transformed into the desired hollow architectures. In this process, the MOF participates directly in forming the hierarchical structure while serving as the template framework. In contrast to the previous two methods, the merits of the self-template method are as follows: (1) it obviates the need for template removal, thereby enhancing synthesis efficiency, reducing production costs, and facilitating scalability. (2) Utilizing MOFs with diverse structures as templates and modulating reaction conditions, this method enables precise control over the size, morphology, spatial distribution, and pore structure of the resulting hollow architectures. With higher flexibility and adaptability, the self-template method is now widely used in preparing complex hierarchical MOF materials, which has great application prospects in the electrochemical energy storage field.

Despite the successful synthesis of some hollow structures, the majority of reported architectures are still limited to simple spherical morphologies. In contrast, complex multi-shell hollow architectures offer enlarged internal voids and higher specific surface areas, which effectively alleviate volume variation during prolonged cycling and significantly enhance structural integrity.[90–92] Building on these structural merits, Lou's group pioneered multi-shell architectures for advanced energy storage applications. For instance, ZIF-67 nanocubes were reacted with selenium powder under controlled annealing to form CoSe@carbon nanoboxes with inhomogeneous shells.[93] The structural evolution is governed by the Kirkendall effect, characterized by the rapid outward diffusion of cobalt ions, contrasting with the slow inward diffusion of selenium. This differential diffusion kinetics leads to the formation of hollow interiors and compositional stratification within the shell, resulting in a CoSe-enriched inner region confined within a carbon-rich outer layer. These structural features effectively buffer lithiation-induced strain while facilitating efficient ionic and electronic transport, thereby enhancing rate performance and cycling stability. Subsequently, leveraging the same template, Lou's group engineered shell multiplicity by modulating vanadium oxytriisopropoxide (VOT) concentration. Through a solvothermal reaction followed by thermal annealing, triple-, double-, and single-shelled Co_3O_4@$Co_3V_2O_8$ nanoboxes were synthesized (Fig. 3c–f).[78] A key mechanistic insight involves VO_4^{3-} ions undergoing ion exchange with 2-methylimidazole ligands in ZIF-67, forming amorphous $Co_3V_2O_8$ (a-$Co_3V_2O_8$) intermediate shells. Electrochemical evaluations of LIB anodes revealed superior performance for triple-shelled nanoboxes, directly attributable to their elaborate frameworks. In addition, the decreased particle size of these MOF-derived materials—compared to earlier systems—shortens the diffusion distance for lithium-ion insertion/extraction, and the multi-shell architecture facilitates close interfacial contact with the electrolyte. It is particularly noteworthy that precise control of the shell number was achieved by modulating the dosage of reactants, offering an

effective synthetic strategy for the controllable synthesis and morphological tailoring of multi-shelled structures.

Self-templating synthesis combined with high-temperature pyrolysis offers a controllable route to fabricate carbon-encapsulated hollow structures, effectively boosting electrode conductivity and rate capability.[94,95] Crucially, the resulting robust carbon shell serves as a protective layer to mitigate volume fluctuations during electrochemical cycling. This self-templating approach further provides a versatile platform for synthesizing diverse electrode materials featuring protective carbon architectures.[96] Extending this strategy, the integration of high-temperature sulfidation and calcination processes facilitates the preparation of MOF-derived TMOs possessing intricate hierarchical morphologies.[97–99] These TMOs are particularly attractive for energy storage due to their natural abundance, high theoretical capacity, and favorable rate performance. Notably, Lou and co-workers engineered CoO/Co–Cu–S hierarchical tubular heterostructures (HTHSs), integrating hollow features within a tubular framework for supercapacitor applications.[79] Specifically, this hierarchical hollow nanotube architecture minimizes ion/electron diffusion distances and significantly improves tolerance to volume variations during charge/discharge processes.

The self-template strategy relies critically on the rational design of precursor architectures coupled with precise control over thermal treatment and etching parameters. Compared to conventional templating strategies, this approach enables more versatile and efficient fabrication of hierarchical architectures, significantly ensuring high-purity products by eliminating template introduction and removal steps. Moreover, the self-templating method utilizes the inherent structure of MOFs as a template, which ensures structural homogeneity with the target architecture and enhances the stability of the modified material.

Overall, in the hard-template method, materials such as PS and SiO_2 are introduced as rigid scaffolds to construct hollow structures with well-defined dimensions and precise architectures. However, the removal of these templates often requires harsh chemical conditions, which may compromise the structural integrity of the resulting hierarchical MOFs. In contrast, the soft-template approach employs removable surfactants or biomolecules under relatively mild conditions, thereby minimizing detrimental effects on the MOF. More advantageously, the self-template strategy eliminates the need for template removal entirely, as the sacrificial precursor itself is transformed or consumed during synthesis, effectively avoiding any exogenous reagents and preserving the stability of the resulting core–shell or hollow structures.

2.1.2 Additive-assisted modulation method. The additive-assisted modulation method has emerged as a pivotal and innovative pathway for constructing hierarchical MOF-based electrode materials, demonstrating exceptional capability in precisely engineering critical morphological and structural attributes.[100] Specifically, it governs the crystal growth kinetics through the introduction of additives that tune the pH or coordination environment, thereby directing the formation of MOF crystals with tailored morphology and dimensions. Typically, these methods exert control over the crystal growth orientation *via* kinetic modulation, enabling the synthesis of MOFs exhibiting distinct morphologies.

By employing ammonia as an additive in a bottom-up approach, Liu *et al.* synthesized M-DBH (M = Ni, Mn, Co) c-MOFs, which utilized 2D conductive MOFs with a 3D extended molecule as electrode materials for lithium storage for the first time.[101] Additionally, the innovative potential of this strategy is vividly illustrated by the work of Shi *et al.* They pioneered nitrogen-rich triptycene-based 2D c-MOFs with vertical extension (Fig. 3g and h).[80] Notably, this work addressed the low yield and crystallinity of Mn-based MOFs by selecting specific basic additives. This led to the synthesis of nitrogen-rich triptycene-based 2D c-MOFs (M-TH5) with dual redox-active centers. Crucially, by simply varying the additive, they achieved precise morphological control: flower-like Mn-TH5 *versus* sheet-like Co-TH5 (Fig. 3i and j). This flower-like Mn-TH5 architecture offers a larger specific surface area and more fully exposed active sites, providing a novel strategy for modulating electrochemical performance. Alternatively, acidic additives can also be taken to modulate the structure of MOF materials.[102] Wang *et al.* developed tunable core–shell PBAs through an acidic additive-mediated synthesis strategy, effectively mitigating structural instability and defect formation during large-scale synthesis of PBAs.[81] This work utilizes a simple one-step synthesis approach to overcome the poor lattice matching and structural collapse often caused by traditional multi-step methods, which is appropriate for large-scale applications. Furthermore, it clarifies the formation mechanism of PBA core–shell structures. Additionally, the strategic introduction of additives enables the rational design of hierarchical MOF architectures with tailored dimensions. Zheng and coworkers chose PVP as an anion surfactant to formulate ultrathin 2D Co-MOF nanosheet structures.[103] This ultrathin nanosheet architecture, with a theoretical thickness of 1.941 nm, exhibits significantly reduced ion diffusion pathways and increased active site density compared to bulk and micron-scale Co-MOF counterparts. Surprisingly, adding additives can even be applied to enhance the stability and synthetic efficiency of MOF materials. Zhou *et al.* fabricated well-dispersed 2D-CuBDC-MBA nanosheet structures with a yield of 88.6% by adding 4-methoxybenzoic acid (MBA) as a modifier.[104] The innovative aspect is the use of a monodentate linker (MBA) to compete with the primary ligand (BDC) for metal coordination. This competition effectively modulates the growth kinetics, leading to improved crystallinity, stability, and colloidal dispersion—factors critical for practical processing and electrode material fabrication.[105]

In conclusion, additives are frequently used to design hierarchical materials with specific geometrical dimensions and architectures. While the additive-assisted synthesis method demonstrates notable advantages in procedural

simplicity, its full potential remains underexplored, warranting systematic investigation into scalability and practical applications. Additionally, future research should focus on elucidating the precise mechanistic roles of additives and further exploring their potential to unlock next-generation MOF architectures with unparalleled performance for advanced electrochemical energy storage.

2.1.3 Etching method. Chemical etching enables precise structural modulation of materials through targeted dissolution, thereby optimizing their functional properties. Based on distinct mechanisms, this approach is categorized into competitive coordination etching and interior core etching.[67] The former involves introducing competitive modulators to disrupt metal–ligand coordination bonds, triggering dissolution–recrystallization equilibria that yield hollow architectures. The interior core etching technique often employs a surface protection strategy to introduce acid reagents such as tannin (TA) and gallic acid (GA) that act as both protected and etching reagents. These reagents protect the structural stability of MOF crystal surfaces and etch the internal structure with more defects, enabling the construction of well-defined hollow structures with preserved crystallinity. Notably, the pH sensitivity of specific MOF families dictates their suitability for this method: ZIFs are susceptible to acidic etchants, Ni(II)-MOF requires alkaline conditions, and UiO-66 can be etched through a "ligand exchange" mechanism.[106,107]

Based on the conventional yolk–shell structure, which typically suffers from limited contact points between the yolk and the shell, Gan *et al.* employed an interior core etching strategy to construct a unique yolk–shell NiS_2@C@C composite.[108] Specifically, TA etching generated internal voids within the ZIF-8 layer, while sequential HCl treatment and calcination yielded dual-carbon-encapsulated yolk–shell architectures. Building on the same approach, Lou *et al.* further developed a Co_3O_4/carbon composite featuring highly dispersed sub-20 nm hollow nanoparticles embedded within mesoporous carbon nanobox walls (H-Co_3O_4@MCNBs).[82] This effectively addresses the issue of non-uniform distribution of TMOs within porous carbon matrices. As illustrated in Fig. 3k, H^+ ions from tannic acid selectively coordinated with Co^{2+} nodes in ZIF-67, forming TA–Co complexes. This ligand substitution mechanism is broadly applicable to various MOF systems, underscoring the scalability and reproducibility of the etching strategy for constructing hollow structures with tailored compositions. The etching strategy has been further extended to MXene-based composites, leveraging their negatively charged surfaces for electrostatic-driven MOF growth and subsequent etching, representing an innovative cross-material integration that enhances conductivity and structural diversity.[109–113] Liu *et al.* demonstrated time-dependent etching control, obtaining MXene@ZIF-67 core–shell cobalt hydroxide (MXene@CS-ZCH), MXene@ZIF-67 yolk–shell cobalt hydroxide (MXene@YS-ZCH), and MXene@ZIF-67 hollow cobalt hydroxide (MXene@HO-CH) derivatives.[114] It innovatively enabled precise temporal control over the morphological evolution of core–shell structures.

Collectively, etching provides a strategic approach for precise structural engineering of both surface and internal architectures within MOFs and their derivatives, thereby enhancing active site density. Specifically, hollow structure dimensions can be precisely tailored by controlling etchant concentration, time, and competitive modifier selection. According to the different MOF precursors, the corresponding etchant can be adopted, and attention should be paid to precisely controlling the reaction conditions to facilitate the exquisite modulation of their morphology.

2.1.4 Ion exchange method. The ion exchange method enables substitution of metal nodes or organic ligands in MOFs, triggering structural reconstruction that often culminates in hierarchical hollow architectures governed by diffusion kinetics and thermodynamics. Thermodynamically controlled ion exchange occurs when the target ion exhibits a higher binding affinity than the host ion, typically achieved through elevated concentration gradients. Kinetically controlled processes, conversely, arise from differential diffusion rates between outgoing and incoming ions. This asymmetry initiates structural reorganization, leading to hollow morphology development *via* accelerated outward diffusion of native ions relative to incoming species. This phenomenon aligns with the Kirkendall effect, as demonstrated in MOF reconstruction processes. Consequently, ion exchange serves as a versatile strategy to tailor the structural and electronic properties of MOFs through direct cation/anion substitution. Critically, this technique achieves atomic-scale precision in framework modification while preserving crystallinity, offering distinct advantages over conventional synthesis routes.[115,116]

By leveraging this ion exchange strategy, Lou's group synthesized diverse hierarchical hollow structures, enabling precise nanostructural modulation of MOF-derived materials.[117–120] For instance, they successfully prepared hierarchical Cu-doped $CoSe_2$ (Cu–$CoSe_2$) microboxes *via* diffusion-driven sequential ion exchange (Fig. 3l).[84] Due to the small size of cobalt ions, outward diffusion of cobalt ions is dominant compared to inward diffusion of Se^{2-} and the selenation reaction occurs on the surface of $CoSe_2$ to form a hollow structure. The second exchange process is based on the same mechanism. Notably, precise modulation of reaction conditions in ion exchange engineering enables the controlled synthesis of multishell architectures. Lou *et al.* developed a strategy to precisely control the shell number of cobalt-based nanoboxes through a multistep ion exchange process combined with solvent temperature regulation.[121] This work offers a general platform for the synthesis of a broad range of MOF-derived materials with precisely tunable multi-shelled structures.

This straightforward, efficient, and eco-friendly ion exchange strategy provides a novel approach to designing and preparing intricate hierarchical materials, which enables rapid ion exchange while simultaneously preserving the

crystallinity of the hierarchical structure. Moreover, the structural integrity and compositional tunability of these MOF-derived architectures significantly enhance their stability and scalability, which are critical for practical electrochemical energy storage applications.

2.2 Synthesis strategies of hierarchical compositional structures

2.2.1 Self-assembly method. The self-assembly strategy represents a bottom-up approach for spontaneously organizing discrete components into one-dimensional (1D), two-dimensional (2D), or three-dimensional (3D) ordered architectures.[122] Crucially, this technique enables precise control over the size, morphology, and interfacial arrangement of hierarchical materials through rational selection of structural modifiers, such as surfactants or ligands.[123] This fine-tuned control, coupled with the inherent advantages of simplified synthesis steps, lower cost, and easier scalability compared to alternative methods, makes self-assembly particularly attractive for fabricating functional MOF-based electrodes.

Hierarchical compositional structures can consolidate the merits of micro- and macro-level architectures. Adopting a multiscale design of hierarchical heterostructured materials plays a crucial role in enhancing the electrochemical performance. Xu and coworkers reported a facile and scalable self-assembly process and successfully prepared novel graphene-wrapped Co,N double-doped mesoporous TiO_2/C frameworks (CN-TC@FG) (Fig. 4a).[85] The co-doped amine-functionalized Ti-MOF precursor doped with TiO_2 nanoparticles is positively charged, which can spontaneously attract negatively charged graphene oxide (GO) for self-assembly to form a 3D heterogeneous network framework structure. This multi-scale design approach based on MOF derivatives integrates the electrochemical merits of diverse structures and holds great promise for synthesizing advanced electrode materials. Recently, with the same method, Wang's group utilized the interfacial interaction of reduced graphene oxide (RGO) to induce the oriented growth of flower-like Ni-MOFs on its surface, designing high-performance supercapacitors.[124] This hierarchical heterostructure combines the abundant active sites of Ni-MOFs and the high conductivity merit of RGO. Meanwhile, it was revealed that the morphology of the hierarchical compositional structure could be controlled by regulating the reaction conditions, including time, temperature, and the amount of RGO added. This strategy, which employs conductive scaffolds as both substrates and structure-directing agents to guide MOF self-assembly, enables the development of hierarchical heterostructures through expanded synthetic pathways. Besides graphene, emerging two-dimensional conductive materials such as MXenes can also be employed to fabricate hierarchical composite materials.[125,126]

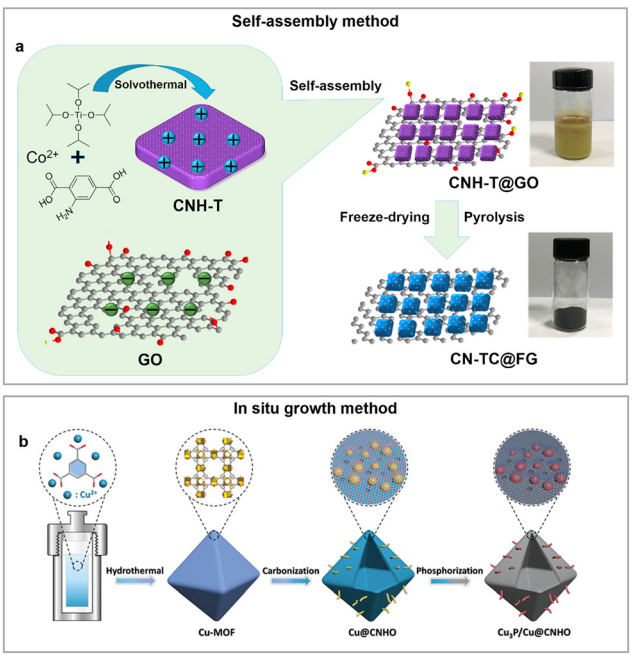

Fig. 4 Some typical synthesis strategies of hierarchical compositional structures: (a) schematic diagram of the CN-TC@FG heterostructure; reproduced with permission from ref. 85. Copyright 2018, Elsevier. (b) Schematic diagram of the CNT-assembled micro/nanostructured Cu_3P/Cu@CNHO heterostructure; reproduced with permission from ref. 86. Copyright 2020, Wiley-VCH.

The self-assembly method enables precise control over the morphology and dimensions of target materials through the selection of different structural units. Moreover, by tailoring both structural and compositional features, hierarchical heterostructures can be constructed to meet diverse functional requirements. Nevertheless, achieving structurally stable assemblies remains challenging, necessitating stringent control over synthesis conditions to prevent morphological degradation.

2.2.2 *In situ* growth method. The *in situ* growth strategy enables the direct construction of functional architectures on MOF substrates or the formation of MOF-based matrices on pre-designed structures. This technique, characterized by interfacial bonding between components, enables precise configuration of composite electrodes through site-specific material integration.

Leveraging their high surface area and tunable porosity, MOFs have emerged as innovative precursors for constructing porous carbon-encapsulated micro/nano heterostructures *via in situ* methods. For instance, Shi and coworkers designed a novel architecture confining FeP quantum dots within a P-doped octahedral carbon framework integrated with carbon nanotubes (FeP@OCF/CNTs).[127] This was achieved through an *in situ* reductive phosphatization/carbonization process of a pre-synthesized MIL-101@CNT precursor, ensuring uniform dispersion of the FeP quantum dots within the three-dimensional carbon host. Crucially, the *in situ* growth of carbon nanotubes on the MOF-derived octahedron surface established efficient pathways for electron transport. Compared with previous studies, this work achieves the

confined growth of FeP quantum dots, the construction of a P-doped three-dimensional porous octahedral framework, and the *in situ* growth of carbon nanotubes simultaneously *via* a one-step phosphatization/carbonization process. Additionally, Lin *et al.* reported a micro/nanostructured Cu_3P/Cu heterostructure encapsulated within a carbon-nanotube-assembled hierarchical octahedral carbonaceous matrix (Cu_3P/Cu@CNHO).[86] Their approach involved the solvothermal synthesis of a Cu-MOF, followed by carbonization under an inert atmosphere to form a porous carbon framework. During this carbonization step, carbon nanotubes were self-generated and assembled on the framework. Subsequent phosphidation of this intermediate yielded the final Cu_3P/Cu@CNHO heterostructure (Fig. 4b). Collectively, these two examples showcase distinct yet sophisticated hierarchical heterostructures derived from MOFs, demonstrating the scalability of this method. The *in situ* formation of interconnected carbon networks, particularly the integrated CNTs in both cases, plays a pivotal role in significantly enhancing electron transport efficiency within these electrode materials.

The *in situ* growth method enables hierarchical compositional control through multi-step precursor template construction, where the precise design of the precursors and the modulation of the conditions of the multistep reaction are key to controlling the hierarchical compositional structure.

2.3 Synthesis strategies of hierarchically porous structures

Hierarchical porous architectures are predominantly fabricated through templating or etching strategies. This section focuses specifically on representative hierarchical porosity structures to highlight recent innovations in structural control and their implications for electrochemical energy storage.

Recently, 3D-ordered MOF single crystals have demonstrated significant potential for material modification due to their high structural regularity, offering a promising strategy for efficient energy storage.[128,129] Yu's group reported 3D-ordered ZIF-8 (3DOM-ZIF-8) derived N-doped hierarchical porous carbon (N-HPC) for KIB anode materials.[65] The synthesis involved PS nanospheres assembled into a highly ordered 3D structure serving as a sacrificial template (Fig. 5a). Subsequently, the ZIF-8 precursor solution infiltrated the interstitial spaces of the PS template, leading to *in situ* crystal growth. Following template removal, the 3DOM-ZIF-8 monolith was obtained. This macroporous MOF precursor was then carbonized under an inert atmosphere to yield the N-HPC material. The resulting N-HPC exhibited a macroporous nanostructure with interconnected pores averaging ~170 nm in diameter (Fig. 5b and c). This structurally ordered architecture significantly reduces ion diffusion distances and mitigates concentration polarization, leading to superior rate capability and cycling stability—a notable advancement over conventional amorphous carbon

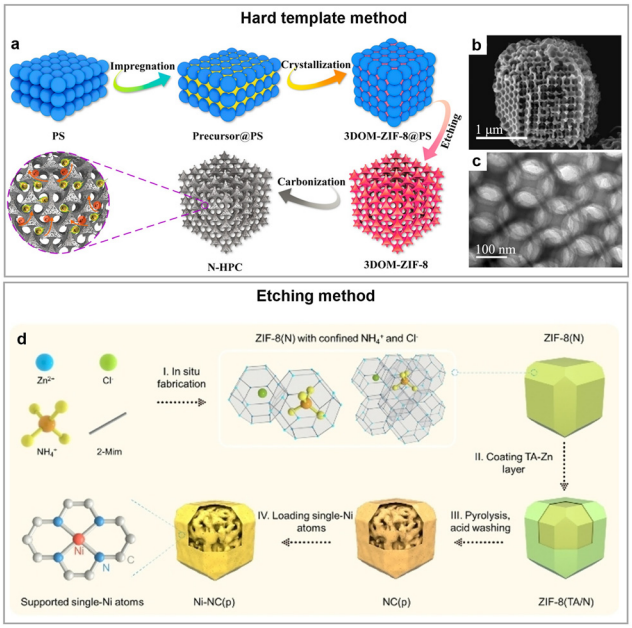

Fig. 5 Some typical synthesis strategies of hierarchical porous structures: (a) schematic diagram of N-HPC; (b) SEM image of N-HPC; (c) TEM image of N-HPC; reproduced with permission from ref. 65. Copyright 2019, American Chemical Society. (d) Schematic illustration of the preparation route for Ni–NC(p); reproduced with permission from ref. 83. Copyright 2022, Wiley-VCH.

materials. In another innovative approach, Sun *et al.* utilized silica nanospheres as a hard template to construct a 3D-ordered MOF-derived carbon network integrated with *in situ*-grown carbon nanotubes. The multi-step process—including solvent evaporation, carbonization, and etching—resulted in a hierarchically porous conductive framework with enhanced charge transfer kinetics.[130] Chemical etching represents another effective strategy for creating hierarchical porosity within MOF-derived carbon materials. Lou and coworkers employed an *in situ* etching strategy during pyrolysis to fabricate mesoporous N-rich carbon decorated with atomically dispersed Ni sites (Ni–NC(p)) (Fig. 5d).[83] The resultant mesoporous structure facilitates efficient ion transport, while the atomically dispersed Ni species significantly enhance the redox kinetics of lithium polysulfides (LiPSs). Encapsulated with NH_4Cl, ZIF-8(N) was fabricated with TA through a chemical etching method to synthesize a complex ZIF-8(TA/N) with a rhombic dodecahedral morphology. Subsequent thermal treatment introduced Ni atoms, resulting in a porous network structure of Ni–NC(p).

Collectively, these studies demonstrate that controlled strategies, whether through hard templates or etching reagents, provide versatile and powerful avenues for engineering complex hierarchical architectures within MOF-derived materials, offering significant potential for advanced energy storage applications. Although numerous studies have focused on synthesizing MOFs with hierarchically porous structures exhibiting diverse morphologies and tunable pore

sizes, the existing synthetic strategies are often limited to producing materials with specific structural features, and a universal methodology remains to be further developed.

2.4 Evaluation criteria for the stability and electrochemical cycling longevity of hierarchical MOFs

The stability of pristine MOFs under diverse environmental conditions is a decisive factor for the rational construction of hierarchical architectures. In terms of hydrolytic resistance, UiO-66(Zr) and MIL-101(Cr) remain intact in aqueous solution for over two months.[131] Additionally, MOFs assembled from high-valence metal ions and carboxylate ligands—including MIL-100(Cr), MIL-53(Cr), UiO-66-NH_2, PCN-222(Fe), and PCN-224—exhibit excellent water stability. Stabilized by inert Zn–N coordination bonds, ZIF-8 also shows remarkable resistance to hydrolysis.[132] Regarding acid–base environments, general trends emerge: MOFs containing high-valence metal ions with carboxylate linkers typically withstand acidic media, whereas those composed of low-valence ions and azolate linkers are more stable under alkaline conditions. Notable examples exhibiting acid tolerance include UiO-66(Zr), UiO-66-NH_2, PCN-222, and MIL-101(Cr), whereas ZIF-8, PCN-601, and MIL-53(Al) demonstrate strong alkaline durability.[133] Such insights into intrinsic stability provide valuable guidance for the design of etching strategies aimed at generating hierarchical porosity and hollow structures.

Representative hierarchical morphologies include yolk–shell, multi-shelled, and single-shelled frameworks. Yolk–shell and multi-shelled systems exhibit superior mechanical integrity and electrochemical endurance, since interlayer voids mitigate volume expansion during cycling.[134] These architectures provide enlarged surface areas, abundant active sites, and shortened ion transport pathways, enabling both high-rate performance and long cycle life. In contrast, single-shelled analogues are generally less robust, whereas multi-layered configurations benefit from cooperative shell effects. Performance optimization, however, requires careful regulation of the shell number and thickness.[135] The stability of hierarchical heterostructures requires careful consideration of the properties of each constituent phase, typically comprising MOF-derived metal oxides, carbides, sulfides, and phosphides. Metal carbides offer high electrical conductivity and chemical robustness, though defect engineering or core–shell motifs are required to enrich active sites.[136] Oxides, sulfides, selenides, and phosphides deliver high theoretical capacity and low redox potential, yet they typically suffer from inferior conductivity and structural degradation due to pronounced volume expansion.[137] Strategies such as constructing two-dimensional nanosheet assemblies or encapsulating with carbon shells are frequently applied to suppress pulverization and improve durability. For hierarchical porous structures, the introduction of mesopores into microporous MOFs containing divalent metal elements often compromises their chemical and thermal stability due to the increased density of defect sites. In contrast, the structural stability of high-valence metal-based MOFs remains largely unaffected under similar modifications. Therefore, it is necessary to control the proportion and distribution of the introduced mesopores and macropores to improve the electrochemical performance while avoiding the introduction of too many defects, resulting in reduced thermal and chemical stability.[138]

The stability of these MOF materials is quantitatively assessed through a suite of experimental techniques. The preservation of crystallinity is routinely confirmed by powder X-ray diffraction after exposure to harsh conditions. The structure can be directly observed by scanning electron microscopy (SEM) and transmission electron microscopy (TEM). The retention of porosity and surface area is evaluated using nitrogen sorption isotherms.[143] Notably, for electrochemical performance, the lifetime is directly measured through long-term cycling tests within devices, where capacity retention over hundreds or thousands of cycles serves as a key metric of operational stability. Additionally, rate capability testing probes the mechanical and chemical stability of the electrode architecture by subjecting it to varying current densities. A high capacity performance recovery upon returning to a low current rate after high-rate cycling is a key indicator of exceptional stability. The specific electrochemical performance analysis will be introduced in detail in the next section.

3. Applications in electrode materials

3.1 Batteries

The rising demand for higher-performance electric vehicles and portable electronic devices, and continuous government attention to low-carbon energy technologies have motivated extensive research into advanced energy storage devices.[144–146] Notably, the structural diversity and tunability of MOFs and their derivatives open up entirely new avenues for the design of electrochemical energy storage systems.

However, the realization of this potential is contingent upon electrochemical performance in practical electrode applications. This performance is typically evaluated by core parameters such as cycling stability, rate capability, and electrical conductivity. However, pristine MOFs exhibit suboptimal cycling stability, which typically sustains <200 cycles for cathodes[147–155] and <500 cycles for anodes.[156–160] Additionally, they induce severe polarization at high current densities due to limited conductivity. Hierarchical structural engineering has been implemented to mitigate these issues: (i) hollow architectures with interior voids accommodate volume changes, while robust shells prevent electrode pulverization; (ii) multiscale porosity shortens ion diffusion distances; (iii) the integration of hierarchical MOFs with highly conductive networks synergistically combines structural benefits with enhanced electrical conductivity. Consequently, hierarchical structuring represents a highly promising strategy for developing high-performance MOF-

Table 2 Electrochemical performance of hierarchical MOFs and derivatives for electrode materials

Sample	Application	Current density	Capacitance [mAh g^{-1}]	Cycle number	Reference
pSiMS@C	LIB-anode	1 A g^{-1}	1027.8	500	5
Co/Fe-based PBA@xBQ	LIB-anode	0.5 C	467.6	500	139
Quasi-Cu-MOF	LIB-anode	0.5 A g^{-1}	514.6	400	140
Cu–HPC	LIB-anode	3 A g^{-1}	1427.4	1000	7
NiSe@C	SIB-anode	3 A g^{-1}	160	2000	8
ZnSe@$CoSe_2$	SIB-anode	5 A g^{-1}	520	500	4
CoHCF@FeHCF	SIB-cathode	0.17 A g^{-1}	111.9	100	141
AC@CoP/NCNTs/CNFs	KIB-anode	0.8 A g^{-1}	247	1000	9
NPC/Cu	KIB-anode	2 A g^{-1}	129	20 000	10
CoMn–PBA HSs	AZIB-cathode	0.05 A g^{-1}	128.6	1000	11
CuMn–PBA DSNBs	AZIB-cathode	0.1 A g^{-1}	116.8	2000	12
DHPBA–Fe(II)	AZIB-cathode	1 A g^{-1}	92.5	10 000	142
S@Ni/Fe LDH	LSB-cathode	1 C	501	1000	13
CoS/HNC-S	LSB-cathode	1 C	455	800	14

based electrodes. This is evidenced by the typically reported capacity retention exceeding 70% even after 100–2000 cycles, alongside excellent rate performance maintained under high-rate conditions. To illustrate these points concretely, this section provides specific applications of hierarchical MOFs and their derivatives across various battery systems such as lithium-ion batteries (LIBs), sodium-ion batteries (SIBs), potassium-ion batteries (KIBs), aqueous zinc-ion batteries (AZIBs), lithium–sulfur batteries (LSBs), and supercapacitors (SCs), with corresponding electrochemical properties summarized in Table 2.

3.1.1 LIBs. The operation of lithium-ion batteries relies on reversible redox reactions involving lithium-ion intercalation/deintercalation at electrodes. Since their commercialization in the 1990s, lithium-ion batteries have emerged as predominant energy storage devices owing to their high energy density and portability.[161,162] However, intrinsic limitations persist in optimizing their electrochemical performance: (1) significant volume variation during Li^+ insertion/extraction induces mechanical stress and capacity fading.[163–165] (2) Limited ionic/electronic conductivity restricts rate capability.[166] (3) Unstable solid-electrolyte interphase (SEI) formation from electrolyte decomposition accelerates performance degradation.[167,168] To address these constraints, hierarchical structural engineering has been implemented to mitigate these issues.

Toward resolving the significant capacity degradation and detrimental interfacial side reactions inherent to silicon anodes, Wang *et al.* first engineered a porous silicon microsphere@carbon (pSiMS@C) core–shell composite *via in situ* MOF coating.[5] It is remarkable that the core of this structure consists of uniquely interconnected nanowires. Additionally, the relationship between the microstructure and lithium-ion storage performance has been clarified. As illustrated in Fig. 6a, the hierarchical core–shell structure integrates a rigid MOF-derived carbon shell with an internal porous silicon network, which synergistically enhances electrochemical kinetics and mechanical stability. Specifically, the rigid MOF-derived carbon shell confining the internal silicon nanowires effectively accommodates volume variation (almost 300%) during cycling. Furthermore, the conductive carbon shell promotes a stable SEI layer, thereby suppressing electrolyte decomposition and improving cycling stability. Remarkably, the pSiMS@C electrode delivers a reversible capacity of 1027.8 mAh g^{-1} after 500 cycles at 1 A g^{-1}, with 79% retention relative to its initial capacity (Fig. 6b). Additionally, it maintains 499.9 mAh g^{-1} at 4.0 A g^{-1}

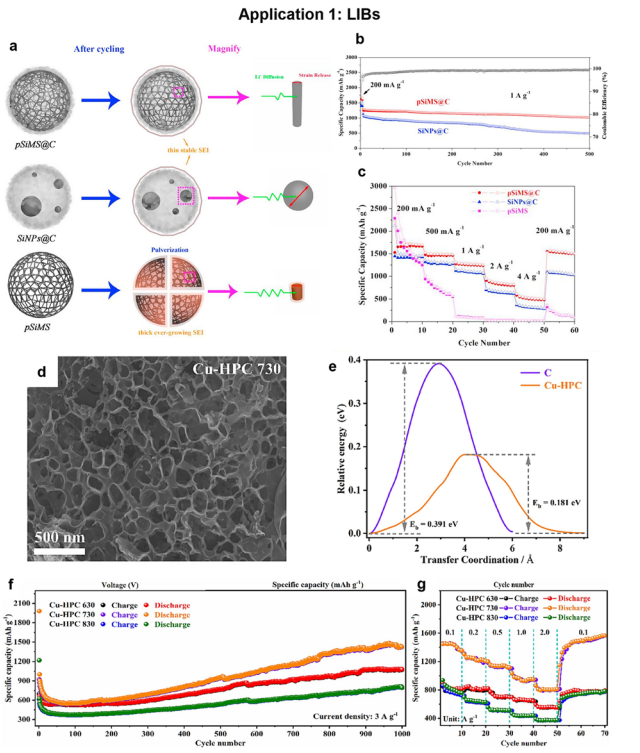

Fig. 6 The applications of hierarchical MOFs and derivatives in LIBs: (a) schematic illustration for lithium storage performances and electrochemical kinetics of pSiMS, SiNPs@C, and pSiMS@C samples. (b) Long-term cycling performances of SiNPs@C and pSiMS@C at 1 A g^{-1}. (c) Rate performances of pSiMS, SiNPs@C and pSiMS@C. Reproduced with permission from ref. 5. Copyright 2018, Elsevier. (d) SEM image of Cu–HPC 730. (e) Migration energy barrier. (f) Cycling performances of Cu–HPC at 3 A g^{-1}. (g) Rate performance of Cu–HPC. Reproduced with permission from ref. 7. Copyright 2024, Elsevier.

(Fig. 6c), attributed to rapid ion transport through its interconnected pores. This study presents a simple *in situ* corrosion strategy for MOF coating that avoids the unavoidable defects of the separated MOF phase of ball-milling methods, facilitating the development of diverse multi-level MOF electrode architectures. Building upon the concept of structural design, heterostructures that intimately integrate different functional components offer distinct advantages for ion diffusion. Notably, black phosphorus quantum dots (BQ) encapsulated in PBA have been demonstrated to enhance electrochemical stability in lithium storage.[169,170] Liu *et al.* reported Co/Fe-based PBA@xBQ composites where BQ encapsulation tunes the morphology and pore accessibility.[139] Specifically, optimizing the BQ content transforms cubic Fe–Co PBA into spherical particles, shortening Li^+ diffusion paths. This structural control enables uniform BQ distribution and intimate contact with metal sites, thereby accelerating charge transfer kinetics. Crucially, encapsulating BQ within the pores of Co/Fe-based PBA mitigates the volume expansion typically associated with two-dimensional black phosphorus quantum dots. Furthermore, modulating the BQ loading content enables precise control of the composite's particle size and morphology, which provides a versatile strategy for tailoring hierarchical structures. Besides heterostructures, hierarchical porous carbon materials leverage high surface area and 3D conductive networks to simultaneously enhance ion/electron transport and mitigate mechanical stress.[140] For instance, Zhu *et al.* utilized a molten salt-assisted pyrolysis strategy to synthesize MOF-derived Cu-hierarchical porous carbon (Cu–HPC).[7] This facile method yielded a material with an ultrahigh surface area (607.78 $m^2\ g^{-1}$) and a large pore volume (0.50 $cm^3\ g^{-1}$) (Fig. 6d). This work employs DFT analysis and investigation of electrochemical kinetic behavior to elucidate the capacity enhancement mechanism and lithium storage mechanism of Cu–HPC materials. The uniformly dispersed Cu nanoclusters within the hierarchical porous carbon significantly enhance overall conductivity, while the interconnected pore structure stabilizes SEI formation by accommodating volume changes and facilitating electrolyte infiltration. DFT results show that Cu clusters reduce the Li^+ migration energy barrier to 0.181 eV, significantly lower than the 0.391 eV barrier in carbon (Fig. 6e), enhancing the reaction kinetics. Consequently, Cu–HPC 730 retains 1427.4 mAh g^{-1} after 1000 cycles at 3.0 A g^{-1} in LIBs (Fig. 6f and g). The environmentally benign and cost-effective synthesis of Cu–HPC presents a novel strategy for designing high-performance LIB anodes.

Collectively, through innovative synthesis and structural design, this research advances energy storage materials by crafting core–shell architectures, employing guest encapsulation for synergy, and engineering 3D networks with hierarchical porosity. These strategies address volume expansion, optimize ion transport, and enhance electrical conductivity.

3.1.2 SIBs. Due to the high abundance and relatively lower cost of sodium compared to lithium, SIBs have emerged as a sustainable alternative to LIBs, garnering significant attention in energy storage technologies to reduce costs.[171,172] However, the larger ionic radius and higher molar mass of Na^+ ions impede the reaction kinetics, leading to reduced ion migration rates.[173,174] Similar to LIBs, SIBs face the inherent challenge of volumetric expansion in electrode materials during cycling, which compromises structural integrity and cycling stability. Consequently, there is an urgent need to design and prepare high-performance electrode materials to address these issues.

To overcome these challenges, MOF-derived materials—especially those with carbon-encapsulated nanoarchitectures—have emerged as a promising platform for high-performance SIB anodes, owing to their structural precision, tunable properties, and enhanced stability. Pyrolysis of MOFs can yield graphitic carbon frameworks, significantly enhancing the rapid diffusion of sodium ions. Moreover, the hierarchical structures formed during pyrolysis effectively accommodate volume expansion during sodiation/desodiation cycles. For instance, Xu *et al.* synthesized MOF-derived selenide@carbon heterostructures with diverse morphologies as high-performance SIB anodes *via* a facile selenidation process.[8] Among these, NiSe@C hollow spheres demonstrated exceptional cycling stability, maintaining a capacity of 160 mAh g^{-1} after 2000 cycles at 3 A g^{-1}. This *in situ* carbon encapsulation strategy provides an efficient and straightforward approach for synthesizing various hierarchical heterostructure materials equipped with oxides, sulfides, and phosphides. Similarly, Lin *et al.* fabricated MOF-derived $ZnSe@CoSe_2$ microspheres and $Cu_2Se@CoSe_2$ nanocubes *via* a carbon-encapsulation strategy, which preserved the original MOF morphology and enhanced electrical conductivity (Fig. 7a–d).[4] The conductive carbon framework boosts electrical conductivity, while the well-defined hollow porous architecture facilitates electrolyte penetration and effectively buffers volume variations during sodiation/desodiation. Notably, the $ZnSe@CoSe_2$ microspheres delivered a remarkable capacity of 520 mAh g^{-1}

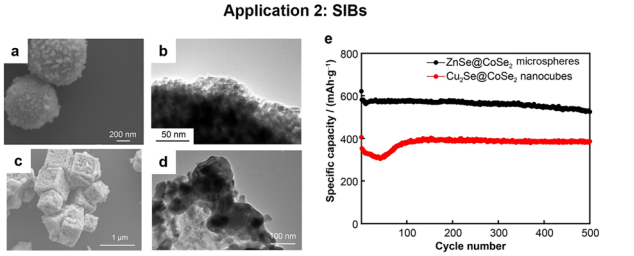

Fig. 7 The applications of hierarchical MOFs and derivatives in SIBs: (a) FESEM image of $ZnSe@CoSe_2$ microspheres; (b) TEM image of $ZnSe@CoSe_2$ microspheres; (c) FESEM image of $Cu_2Se@CoSe_2$ nanocubes; (d) TEM image of $Cu_2Se@CoSe_2$ nanocubes; (e) cycling performances of $ZnSe@CoSe_2$ microspheres and $Cu_2Se@CoSe_2$ nanocubes at 5.0 A g^{-1}. Reproduced with permission from ref. 4. Copyright 2022, Youke Publishing.

after 500 cycles even at an ultrahigh current density of 5 A g^{-1} (Fig. 7e), underscoring the efficacy of this approach. Besides carbon encapsulation, core–shell structural engineering provides another effective strategy to enhance electrochemical performance. Pan *et al.* innovatively designed a CoHCF@FeHCF core–shell cathode. This design strategically utilizes a stable FeHCF shell to protect a high-capacity CoHCF core, creating a synergistic effect that mitigates the individual limitations of each component. This design strategy effectively addresses the persistent issue of capacity degradation in CoHCF under high-rate conditions, as reported in previous studies.[141] Notably, this architecture not only enables refined structural modulation but also leads to synergistic enhancement: the shell ensures excellent rate capability and cycling stability, while the core delivers high capacity, resulting in superior overall performance.

In summary, the novel integration of MOF-derived synthesis with hierarchical structural engineering—through carbon encapsulation, hollow structure design—provides a powerful tool for developing high-performance SIB electrodes. These strategies work in concert to optimize conductive networks, facilitate ion transport, and dissipate mechanical strain, which are crucial for achieving exceptional rate capability and ultralong cyclability. This demonstrates the merits of hierarchical structured materials in electrode materials.

3.1.3 KIBs. Potassium ion batteries (KIBs) have emerged as a promising alternative to lithium-ion systems, driven by the abundance of potassium, its low cost, and a favorable redox potential (K/K^+, −2.93 V *vs.* Li/Li^+, −3.04 V) that enables high energy density.[175] However, the larger ionic radius of K^+ (1.38 Å) compared to Na^+ (1.02 Å) induces sluggish ion diffusion kinetics and severe structural strain during cycling, limiting the rate capability and cycle life.[176,177] The commercial graphite anode material used in lithium-ion batteries is unsuitable for potassium-ion batteries. Therefore, the development of novel anode materials with larger reversible capacity and higher stability has become imperative. In this context, innovative structural engineering using MOFs as precursors has opened new avenues for designing advanced KIB electrodes.

The key breakthrough lies in the ability to construct hierarchically porous, heterogeneous architectures that are difficult to achieve through conventional methods. These MOF-derived structures excel in simultaneously mitigating volume strain, facilitating rapid ion/electron transport, and exposing abundant active sites. For instance, Miao *et al.* pioneered a triple-confined architecture where CoP nanoparticles are spatially constrained within amorphous carbon shells for the first time, which are further embedded in N-doped carbon nanotubes grown on carbon nanofibers (AC@CoP/NCNTs/CNFs).[9] The TEM and HRTEM images indicated that the amorphous carbon shell exhibits excellent mechanical flexibility to effectively mitigate stress caused by volume expansion, while simultaneously imposing spatial confinement on CoP nanoparticles (Fig. 8a–c). Electrochemical profiling (Fig. 8d and e) of AC@CoP/NCNTs/CNFs reveals 81% capacity retention after 200 cycles at 0.1 A g^{-1}, remarkably outperforming pristine CoP (48%) due to suppressed particle pulverization. After 1000 cycles at 0.8 A g^{-1}, the AC@CoP/NCNTs/CNFs still exhibited excellent rate performance with a reversible capacity of 247 mAh g^{-1} (Fig. 8f). Compared with previous relevant studies, this method avoids cumbersome synthetic routes while demonstrating superior performance over other reported CoP-based anode materials. Additionally, introducing heteroatom doping and defect engineering into MOF-derived carbon materials has become an efficient method for developing advanced potassium-ion battery anodes. An *et al.* synthesized N-doped porous carbon on Cu foam (NPC/Cu) *via* ZIF-8 pyrolysis, achieving a graphene-like structure with hierarchical porosity.[10] Consequently, the NPC/Cu anode achieved an ultra-long cycle life that is unprecedented for carbon-based KIB anodes, retaining 129 mAh g^{-1} after 20 000 cycles at 2 A g^{-1} with a minuscule decay rate of only 0.0034% per cycle and near-unity coulombic efficiency. This study pioneered a green, vacuum demetallization-assisted carbonization strategy to fabricate a two-dimensional N-doped hierarchical porous carbon array on a three-dimensional metal substrate, which significantly offers valuable perspectives to construct hierarchical porous materials.

Incorporating heterostructures, hierarchical pores, and core–shell architectures enhances the structural controllability of MOF-based materials. These designs synergize multi-component electrochemical properties at the macro scale and improve ion transport while buffering volume changes at the micro scale. Additionally, the design of MOF-derived metal selenides[178] and sulfides[179] represents a strategic pivot in pursuing high-performance electrodes, offering a versatile platform for optimizing their capacity and cycling stability.

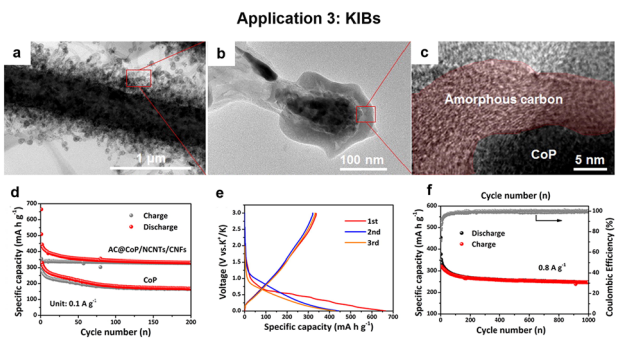

Fig. 8 The applications of hierarchical MOFs and derivatives in KIBs: (a and b) TEM images of the AC@CoP/NCNTs/CNFs sample; (c) HRTEM image of the AC@CoP/NCNTs/CNFs sample; (d) cyclic performance of the AC@CoP/NCNTs/CNFs and pure CoP electrodes at 0.1 A g^{-1}; (e) charging/discharging curves of AC@CoP/NCNTs/CNFs; (f) cyclic performance of the AC@CoP/NCNTs/CNFs electrode at 0.8 A g^{-1}. Reproduced with permission from ref. 9. Copyright 2019, Elsevier.

3.1.4 AZIBs. AZIBs realize the energy storage/release process through reversible Zn^{2+} insertion/extraction reactions at the cathode and dissolution/deposition at the anode.[180] By employing non-flammable aqueous electrolytes and abundant zinc metal anodes, AZIBs have garnered significant attention owing to their inherent safety, high theoretical capacity, low cost, and environmental benignity.[181,182] Consequently, they represent a leading candidate for large-scale energy storage systems.

Notably, the structural design of cathode materials plays a pivotal role in enhancing the electrochemical performance of AZIBs. Lou's group leveraged the high aqueous stability and multi-redox active sites of PBAs to synthesize Co-substituted Mn-rich PBA hollow spheres (CoMn–PBA HSs).[11] The hierarchical hollow structure with a shell thickness of about 200 nm exposes abundant active sites and alleviates volume expansion during cycling. Moreover, partial Co substitution suppresses the Jahn–Teller distortion of Mn–N_6 octahedra, stabilizing the crystal structure and improving cycling stability. The CoMn–PBA HSs achieve 76.4% capacity retention over 1000 cycles at 1 A g^{-1}, confirming the efficacy of Co substitution. This work employs an efficient and straightforward metal substitution strategy *via* a self-templated method to synthesize hollow hierarchical PBA-derived materials. The resulting material exhibits significantly superior performance compared to most reported PBA-based cathodes for aqueous zinc-ion batteries. Furthermore, this approach provides an effective solution to the limited cycling stability of Mn-based PBAs. Extending this strategy, they fabricated Cu-substituted Mn–PBA double-shelled nanoboxes (CuMn–PBA DSNBs) *via* tannic acid etching and cation exchange.[12] Notably, CuMn–PBA DSNBs retain 96.8% capacity after 2000 cycles at 1 A g^{-1}, surpassing Mn–PBA counterparts by >20%. Building on prior work, Zhang *et al.* developed double-shelled PBAs with divalent/trivalent iron (DHPBA–Fe(II) and DHPBA–Fe(III)) *via* an innovative inner–outer growth (IOG) strategy.[142] The IOG mechanism involves lattice-matching-directed epitaxial growth and ligand exchange, as illustrated in Fig. 9(a).

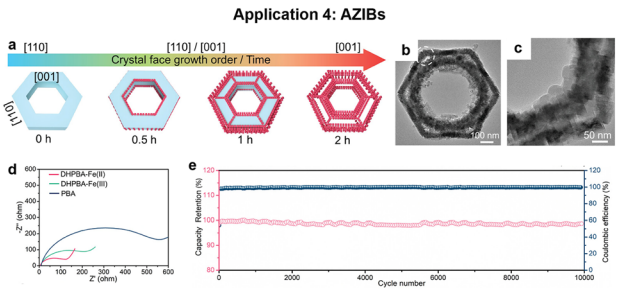

Fig. 9 The applications of hierarchical MOFs and derivatives in AZIBs: (a) illustration of the inner–outer growth mechanism; (b and c) TEM images of DHPBA–Fe(II); (d) Nyquist plots of DHPBA–Fe(II), DHPBA–Fe(III), and cubic PBA; (e) stability test performed at 2 A g^{-1} of DHPBA–Fe(II). Reproduced with permission from ref. 142. Copyright 2023, Wiley-VCH.

DHPBA–Fe(II) possesses a hierarchical porous architecture with an inter-shell spacing of about 30 nm (Fig. 9b), and voids at shell junctions facilitating ion transport (Fig. 9c). This unique architecture enables rapid Zn^{2+} diffusion, as confirmed by low Warburg impedance (Fig. 9d). At 2 A g^{-1}, DHPBA–Fe(II) retains 99.2% of its initial capacity after 10 000 cycles (Fig. 9e). This work utilizes an open architecture as a template to further simplify the synthesis strategy, and the IOG approach for constructing hollow core–shell architectures, thereby enhancing the structural diversity of hierarchical architectural structures. In addition, *in situ* characterization techniques were employed to elucidate the underlying formation mechanism.

While structural innovations in multi-shelled MOFs have extended the cycle life of AZIBs beyond 10 000 cycles, persistent challenges in material scalability, interfacial reactions, and insufficient energy density warrant fundamental investigation and engineering solutions.

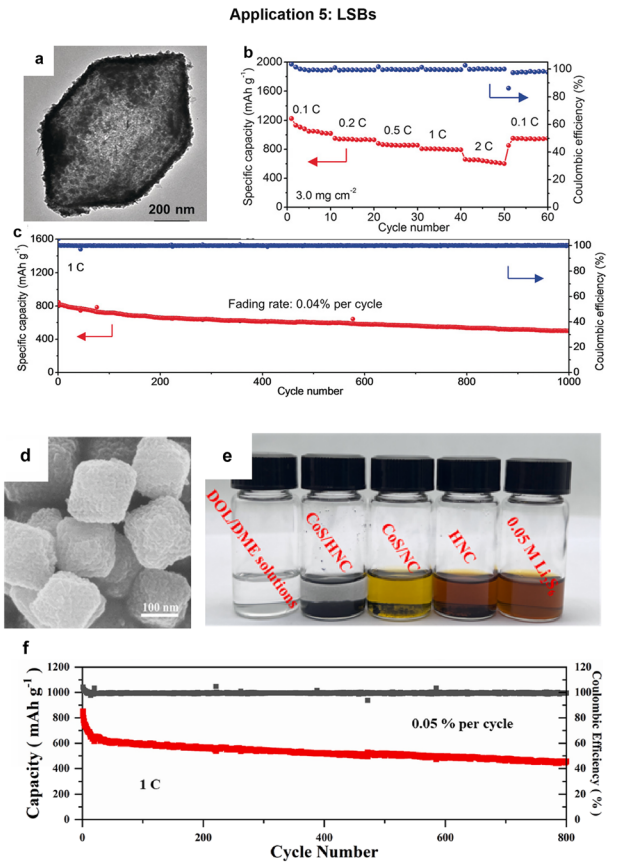

Fig. 10 The applications of hierarchical MOFs and derivatives in LSBs: (a) TEM image of hollow Ni/Fe LDH polyhedra; (b) rate capabilities of S@Ni/Fe LDH at current densities from 0.1 to 2.0 C; (c) prolonged cycle life of S@Ni/Fe LDH at 1.0 C. Reproduced with permission from ref. 13. Copyright 2018, Wiley-VCH. (d) SEM image of UiO-66-NH_2(H); (e) image showing the adsorption capacity tests of CoS/HNC, CoS/NC, and HNC in mixed DOL/DME solutions of Li_2S_6; (f) cycling performance of CoS/HNC-S at 1 C. Reproduced with permission from ref. 14. Copyright 2024, Elsevier.

3.1.5 LSBs. Lithium–sulfur batteries operate through multistep redox reactions between S_8 and Li_2S, involving soluble lithium polysulfide intermediates (Li_2S_x, $4 \leq x \leq 8$), to convert chemical energy into electricity. This redox process involves intricate solid–liquid–solid phase transformations and concomitant ion/electron transfer, governed by complex reaction kinetics.[183,184] Compared to lithium-ion batteries, LSBs offer significantly higher theoretical energy density, positioning them as promising candidates for next-generation energy storage systems.[185,186] Furthermore, sulfur boasts an extraordinary theoretical energy density (2600 Wh kg^{-1}), natural abundance, low cost, and environmental benignity.[187] However, the practical deployment of LSBs faces significant hurdles, including the detrimental polysulfide shuttle effect, limited cycle life, and irreversible structural degradation of the cathode.[188,189] To address these challenges, embedding sulfur into functional host materials with hierarchical hollow structures has become a widely adopted strategy, as they can physically confine polysulfides and provide chemical adsorption sites.

Notably, MOF-derived hierarchical hollow structures not only enhance polysulfide confinement but also improve structural stability due to their tunable porosity and robust frameworks. In a pioneering study, Lou *et al.* designed hollow Ni/Fe LDH polyhedra as a sulfur host (S@Ni/Fe LDH, Fig. 10a), which provided both physical encapsulation and catalytic conversion of polysulfides.[13] This approach overcomes the inherent drawback of diminished electrocatalytic effectiveness due to the physical separation between the catalyst on the separator and the sulfur species in the cathode. Additionally, the Ni/Fe LDH shell kinetically accelerates the redox conversion of long-chain polysulfides to insoluble Li_2S_2/Li_2S, effectively minimizing polysulfide dissolution and mitigating the shuttle effect. The S@Ni/Fe LDH cathode demonstrated excellent rate capability and prolonged cycling stability, delivering a specific capacity of 501 mAh g^{-1} after 1000 cycles at 1 C with a remarkably low capacity decay of only 0.04% per cycle (Fig. 10b and c). Recently, Yao *et al.* proposed an innovative "non-uniform nucleation-growth" strategy to construct hollow MOFs, which were subsequently converted into N-doped hierarchical carbon with embedded CoS nanoparticles (CoS/HNC).[14] Their precursor, H-UiO-66-NH_2, exhibited an octahedral morphology with surface folds and an average size of ~150 nm (Fig. 10d). This design combines a hollow nanostructure to accommodate sulfur volume expansion and CoS nanoparticles, providing abundant polar sites for strong polysulfide adsorption, synergistically inhibiting the shuttle effect. Visual polysulfide adsorption tests using a Li_2S_6 solution revealed that CoS/HNC induced the most significant color change from brown to nearly colorless, outperforming both CoS/NC and HNC controls (Fig. 10e). This design synergistically combines hollow carbon for volume buffering and CoS nanoparticles for strong chemical adsorption and catalytic conversion of polysulfides, effectively suppressing the shuttle effect. The long-term cycling at 1 C showed that the CoS/HNC-S cathode maintained a specific capacity of 455 mAh g^{-1} after 800 cycles, corresponding to an extremely low capacity decay rate of 0.05% per cycle, highlighting its exceptional cycling stability (Fig. 10f). The novel synthesis strategy developed here enables precise control over the composition and morphology of MOF-derived hollow carbon materials, thereby paving the way for the rational design of high-performance lithium–sulfur batteries.

Conclusively, the hierarchical hollow frameworks are designed to accommodate the volume expansion of sulfur and enhance the sulfur loading capacity, while the introduction of heterostructure components provides abundant active sites, thereby promoting polysulfide adsorption and effectively suppressing the polysulfide shuttle effect. Moreover, the design of hierarchical MOF structures must account for the paramount importance of pore size in confining and adsorbing sulfur species. Tailoring the pore size provides an effective strategy to maximize polysulfide loading.

3.2 Supercapacitors

Electrochemical energy storage systems attract significant research interest in hierarchical MOF-based electrodes due to their unique advantage. These devices operate *via* three dominant mechanisms: electric double-layer capacitance (EDLC), pseudocapacitance, and hybrid behavior.[190] The distinct charge-storage pathways necessitate tailored electrode design. Compared to batteries, supercapacitors exhibit higher power density and sub-second charge/discharge capability, making them critical for applications requiring rapid energy bursts, including electric vehicles and the smart grid.[191,192] Central to device performance, electrode materials dictate key metrics: specific capacitance, rate capability, and cycling stability. Hierarchical MOF architectures—featuring tunable porosity and redox-active sites—enable capacitance enhancement, demonstrating viable commercialization pathways.[193,194]

Capitalizing on the dual advantages of high conductivity and abundant active sites in hollow carbon architectures,

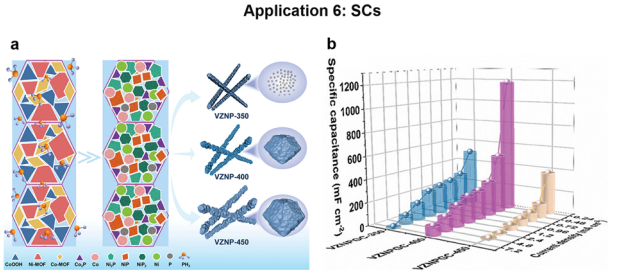

Fig. 11 The applications of hierarchical MOFs and derivatives in SCs: (a) schematic diagram of controllable adjustment of the material morphology by increasing the variety of phosphides through multivalent nickel metal doping; (b) comparison of specific capacitance. Reproduced with permission from ref. 16. Copyright 2024, Wiley-VCH.

Lou *et al.* engineered nitrogen-doped carbon nanofibers composed of interconnected hollow nanoparticles (HPCNFs-N). This one-dimensional design facilitates rapid electron transport and maximizes the electrolyte–electrode contact area.[15] Significantly, this work pioneers a facile electrospinning technique that circumvents the intricate template-removal process inherent to conventional template methods. This strategy establishes a new paradigm for hollow structure synthesis, presenting an elegant alternative to existing techniques. Also based on the ion/electron diffusion benefits of hierarchical hollow structures, Zhou *et al.* synthesized transition metal phosphide composites *via* a low-temperature phosphidation strategy. Using nano-NiCo-MOF (VZN) as a precursor, they preserved the hollow framework while *in situ* generating conductive phosphides (Fig. 11a).[16] Crucially, the introduction of a multivalent metal doping strategy significantly enhanced the structural stability of the nano-MOF composite during the redox process, enabling morphology control through coordination strength modulation. Electrochemical testing revealed that the VZNP-400//MXene asymmetric supercapacitor achieved a remarkable areal capacitance of 1184 mF cm^{-2} at 0.24 mA cm^{-2} (Fig. 11b), attributed to the synergistic effects of hollow MOF-derived phosphides and conductive MXene.

These studies collectively demonstrate that hierarchical hollow architectures coupled with heteroatom doping (N,P) significantly enhance structural robustness and cycling stability, providing design principles for next-generation supercapacitors. Concurrently, the inherent limitations of MOFs, such as their poor chemical/thermal stability and low electrical conductivity, adversely affect cycling stability and mechanical stability. These challenges remain to be effectively addressed through the strategic design of hierarchical heterostructures.

4. Conclusion and perspectives

In conclusion, this review comprehensively outlines synthesis methodologies for hierarchical MOFs and their derivatives, while highlighting recent breakthroughs in their applications for advanced electrochemical energy storage systems, including LIBs, SIBs, KIBs, AZIBs, LSBs, and SCs. By bridging the gap between structural engineering and electrochemical performance, this work provides critical insights into the rational design of hierarchical architectures and their transformative potential in energy technologies.

Compared to conventional MOFs, hierarchical configurations exhibit superior architectural merits: (1) Enhanced porosity and tailored surface chemistry enable exceptional specific surface areas and active site densities, addressing intrinsic limitations such as poor conductivity and mechanical instability. (2) Multi-shell hollow architectures mitigate electrode volume fluctuations through internal stress buffering, thereby improving cycling stability. (3) Hierarchical pore systems synergize micropores, mesopores, and macropores to optimize ion diffusion kinetics while minimizing interfacial resistance, yielding remarkable rate capabilities. (4) Compositional hybridization strategies—such as MOF/carbon composites, MOF/TMP composites, MOF/TMO composites, MOF/TMC composites, MOF/TMS composites, MOF/MXene composites, and heteroatom-doped MOF derivative materials—leverage synergistic interfacial effects to amplify charge transfer efficiency. (5) The integration of multi-scale porosity, architectural complexity, and compositional diversity unlocks unprecedented electrochemical performance through cross-hierarchical coupling effects.

Despite these advancements, critical challenges persist: (1) The precise control over specific hierarchical architectures remains a significant challenge. The precise and controllable synthesis of MOFs with tailored shell layer numbers, pore distribution, and heterostructure assembly remains a significant issue. Mastering these synthetic strategies is crucial for enhancing the performance of MOF-based electrode materials through hierarchical structural engineering. (2) The formation mechanisms and structure–activity relationships of hierarchical MOF materials remain incompletely understood. Further insights urgently require advanced *in situ* characterization techniques, such as *in situ* XRD, microscopy, infrared, and Raman, combined with theoretical calculations. A particular challenge lies in exploring the quantitative correlation between multi-scale structural features—such as pore size hierarchy and shell thickness—with electrochemical performance. (3) The synthesis of sophisticated hierarchical MOFs often involves multi-step processes, which introduce significant uncertainty in the final structure. Moreover, slight variations in key reaction parameters—such as temperature and concentration—may cause substantial structural deviations, thereby compromising reproducibility. (4) Conventional methods such as templating and etching often suffer from stringent conditions and low yield, underscoring the need to develop greener, low-cost, and scalable alternative approaches to finely regulate the morphology, porosity, and composition of hierarchical MOFs and their derivatives. (5) Most hierarchical MOFs are synthesized from MOF precursors. However, the limited variety of conventional MOF platforms—such as ZIFs, PBAs, and MILs—constrains structural diversity. The development of novel MOF precursors is essential to access a broader range of hierarchical architectures. (6) Current research on hierarchically structured MOFs primarily focuses on core–shell configurations and hierarchically porous architectures, while the diversity of hierarchical heterostructures remains limited. For instance, hierarchical architectures derived from MOFs—such as one-dimensional nanoarrays, two-dimensional nanosheets, and three-dimensional nanoflowers—exhibit enhanced mechanical stability and improved ion transport rates, yet these promising morphologies warrant further exploration. (7) Furthermore, systematic studies on the stability of hierarchically porous, architectural, and compositional MOF systems remain insufficient. New strategies must be

developed to mitigate structural collapse induced by volumetric variation during the prolonged cycling process, thereby enhancing the structural stability of hierarchical MOFs.

Based on these analyses, future efforts should prioritize the following: (1) Future research will focus on designing and synthesizing MOF-based electrode materials with increasingly sophisticated and well-defined hierarchical architectures. The goal is to achieve synergistic enhancement of ion transport, mechanical stability, and active site accessibility through the tailored architectures. (2) Another promising direction involves developing multi-functional hierarchical MOFs and their derivatives. Significant efforts will be devoted to creating "bifunctional" or "multifunctional" electrode materials that combine energy storage capabilities with catalytic properties. The integration of multiple functions within a single, structurally optimized material offers a powerful strategy for maximizing overall device performance and enabling new applications in integrated energy conversion and storage systems. (3) It is a promising approach to utilize machine learning to develop hierarchical structure–performance descriptors, which can accelerate the discovery of optimal materials, enabling the efficient identification of key governing factors from complex datasets and the prediction of promising candidate structures from vast chemical spaces.

Author contributions

Zimeng Shao: writing – original draft. Kai Shi: investigation, writing – review & editing. Jiahao Wei: writing – review & editing. Lina Zhou: writing – review & editing. Dandan Han: conceptualization, writing – review & editing, supervision. Junbo Gong: supervision.

Conflicts of interest

There are no conflicts to declare.

Data availability

No primary research results, software, or code have been included, and no new data were generated or analysed as part of this review.

Acknowledgements

This work was supported by the National Natural Science Foundation of China (22208236, 22578315) and the Natural Science Foundation of Tianjin (23JCQNJC01880).

Notes and references

1 J. Lin, X. Zhang, E. Fan, R. Chen, F. Wu and L. Li, *Energy Environ. Sci.*, 2023, **16**, 745–791.
2 W. Zhou, Y. Tang, X. Zhang, S. Zhang, H. Xue and H. Pang, *Coord. Chem. Rev.*, 2023, **477**, 214949.
3 M. A. Hannan, S. B. Wali, P. J. Ker, M. S. A. Rahman, M. Mansor, V. K. Ramachandaramurthy, K. M. Muttaqi, T. M. I. Mahlia and Z. Y. Dong, *J. Energy Storage*, 2021, **42**, 103023.
4 Y.-M. Lin, H.-S. Fan, C.-Z. Zhu and J. Xu, *Rare Met.*, 2022, **41**, 4104–4115.
5 K. Wang, S. Pei, Z. He, L. Huang, S. Zhu, J. Guo, H. Shao and J. Wang, *Chem. Eng. J.*, 2019, **356**, 272–281.
6 X. Liu, M. Yu, S. Wu and J. Gong, *J. Alloys Compd.*, 2023, **969**, 172291.
7 B. Zhu, M. Zhang, Y. Liu, Y. Liu, X. Zhang, Y. Song, L. Wang and R. Mi, *Chem. Eng. J.*, 2024, **482**, 149161.
8 X. Xu, J. Liu, J. Liu, L. Ouyang, R. Hu, H. Wang, L. Yang and M. Zhu, *Adv. Funct. Mater.*, 2018, **28**, 1707573.
9 W. Miao, X. Zhao, R. Wang, Y. Liu, L. Li, Z. Zhang and W. Zhang, *J. Colloid Interface Sci.*, 2019, **556**, 432–440.
10 Y. An, Y. Tian, Y. Li, S. Xiong, G. Zhao, J. Feng and Y. Qian, *J. Mater. Chem. A*, 2019, **7**, 21966–21975.
11 Y. Zeng, X. F. Lu, S. L. Zhang, D. Luan, S. Li and X. W. Lou, *Angew. Chem., Int. Ed.*, 2021, **60**, 22189–22194.
12 Y. Zeng, J. Xu, Y. Wang, S. Li, D. Luan and X. W. Lou, *Angew. Chem., Int. Ed.*, 2022, **61**, e202212031.
13 J. Zhang, Z. Li, Y. Chen, S. Gao and X. W. Lou, *Angew. Chem., Int. Ed.*, 2018, **57**, 10944–10948.
14 Y. Yao, C. Zhou, Z.-L. Zhao, G.-G. Chang, J.-K. Wei, K.-X. Huang, J.-J. Xie, J.-S. Li and X.-Y. Yang, *Carbon*, 2024, **223**, 119018.
15 L.-F. Chen, Y. Lu, L. Yu and X. W. Lou, *Energy Environ. Sci.*, 2017, **10**, 1777–1783.
16 H. Zhou, S. Gu, Y. Lu, G. Zhang, B. Li, F. Dou, S. Cao, Q. Li, Y. Sun, M. Shakouri and H. Pang, *Adv. Mater.*, 2024, **36**, 2401856.
17 R. Zhu, Y. Xu, L. Liu, Y. Jiang, Y. Gu and H. Pang, *Chem. Eng. J.*, 2024, **499**, 156303.
18 Y. Peng, J. Xu, J. Xu, J. Ma, Y. Bai, S. Cao, S. Zhang and H. Pang, *Adv. Colloid Interface Sci.*, 2022, **307**, 102732.
19 R. Zhao, Z. Liang, R. Zou and Q. Xu, *Joule*, 2018, **2**, 2235–2259.
20 X. F. Lu, Y. Fang, D. Luan and X. W. D. Lou, *Nano Lett.*, 2021, **21**, 1555–1565.
21 O. M. Yaghi, G. Li and H. Li, *Nature*, 1995, **378**, 703–706.
22 J. Ha and H. R. Moon, *CrystEngComm*, 2021, **23**, 2337–2354.
23 W. Wang, D. Chen, F. Li, X. Xiao and Q. Xu, *Chem*, 2024, **10**, 86–133.
24 W. Yang, X. Li, Y. Li, R. Zhu and H. Pang, *Adv. Mater.*, 2019, **31**, 1804740.
25 M. Liu, J. Liang, Y. Tian and Z. Liu, *CrystEngComm*, 2022, **24**, 724–737.
26 S. Li, L. Zhao, Y. Yao, Z. Gu, C. Liu, W. Hu, Y. Zhang, Q. Zhao and C. Yu, *CrystEngComm*, 2023, **25**, 284–289.
27 Y. Tong, H. Xu, T. Li, Z. Kong, J. Li, Q. H. Fan, H. Xu, H. Jin and K. Wang, *CrystEngComm*, 2022, **24**, 6944–6952.
28 C. Altintas, I. Erucar and S. Keskin, *CrystEngComm*, 2022, **24**, 7360–7371.

29 R. Abazari, S. Sanati, P. Stelmachowski, Q. Wang, A. Krawczuk, J. Goscianska and M. Liu, *Inorg. Chem.*, 2024, **63**, 5642–5651.
30 J. Liu, Q. Ye, Y. Wu, J. Chen, Y. Ge, L. Zhang, R. Abazari and J. Qian, *Sci. China: Chem.*, 2025, **68**, 1859–1868.
31 S. Sanati, R. S. Varma, M. Liu and R. Abazari, *Energy Environ. Sci.*, 2025, **18**, 7733–7755.
32 R. Abazari, S. Sanati, N. Li and J. Qian, *Inorg. Chem.*, 2023, **62**, 18680–18688.
33 Y. Pan, S. Sanati, R. Abazari, V. N. Noveiri, J. Gao and A. M. Kirillov, *Inorg. Chem.*, 2022, **61**, 20913–20922.
34 Y. Wu, J. Liu, Q. Sun, J. Chen, X. Zhu, R. Abazari and J. Qian, *Chem. Eng. J.*, 2024, **483**, 149243.
35 Y. Zou, Y. Yan, Q. Xue, C. Zhang, T. Bao, X. Zhang, L. Yuan, S. Qiao, L. Song, J. Zou, C. Yu and C. Liu, *Angew. Chem., Int. Ed.*, 2024, **63**, e202409799.
36 P. Fratzl, *J. R. Soc., Interface*, 2007, **4**, 637–642.
37 R. Lakes, *Nature*, 1993, **361**, 511–515.
38 L. Feng, K.-Y. Wang, J. Willman and H.-C. Zhou, *ACS Cent. Sci.*, 2020, **6**, 359–367.
39 Y. Yao, X. Zhao, G. Chang, X. Yang and B. Chen, *Small Struct.*, 2023, **4**, 2200187.
40 L. Zhang, H. B. Wu, S. Madhavi, H. H. Hng and X. W. Lou, *J. Am. Chem. Soc.*, 2012, **134**, 17388–17391.
41 L. Zhang, H. B. Wu and X. W. Lou, *J. Am. Chem. Soc.*, 2013, **135**, 10664–10672.
42 G. Huang, F. Zhang, L. Zhang, X. Du, J. Wang and L. Wang, *J. Mater. Chem. A*, 2014, **2**, 8048–8053.
43 L. Yu, J. F. Yang and X. W. Lou, *Angew. Chem., Int. Ed.*, 2016, **55**, 13422–13426.
44 F. Zou, Y.-M. Chen, K. Liu, Z. Yu, W. Liang, S. M. Bhaway, M. Gao and Y. Zhu, *ACS Nano*, 2016, **10**, 377–386.
45 G. Zhang, S. Hou, H. Zhang, W. Zeng, F. Yan, C. C. Li and H. Duan, *Adv. Mater.*, 2015, **27**, 2400–2405.
46 R. Wu, D. P. Wang, X. Rui, B. Liu, K. Zhou, A. W. K. Law, Q. Yan, J. Wei and Z. Chen, *Adv. Mater.*, 2015, **27**, 3038–3044.
47 G. Huang, F. Zhang, X. Du, Y. Qin, D. Yin and L. Wang, *ACS Nano*, 2015, **9**, 1592–1599.
48 Y. M. Chen, L. Yu and X. W. Lou, *Angew. Chem., Int. Ed.*, 2016, **55**, 5990–5993.
49 F. Zheng, Y. Yang and Q. Chen, *Nat. Commun.*, 2014, **5**, 5261.
50 F. Zou, X. Hu, Z. Li, L. Qie, C. Hu, R. Zeng, Y. Jiang and Y. Huang, *Adv. Mater.*, 2014, **26**, 6622–6628.
51 Q. Wang, R. Zou, W. Xia, J. Ma, B. Qiu, A. Mahmood, R. Zhao, Y. Yang, D. Xia and Q. Xu, *Small*, 2015, **11**, 2511–2517.
52 J. Zhang, H. Hu, Z. Li and X. W. Lou, *Angew. Chem., Int. Ed.*, 2016, **55**, 3982–3986.
53 B. Y. Guan, A. Kushima, L. Yu, S. Li, J. Li and X. W. Lou, *Adv. Mater.*, 2017, **29**, 1605902.
54 P. Zhang, B. Y. Guan, L. Yu and X. W. Lou, *Angew. Chem.*, 2017, **129**, 7247–7251.
55 H. Hu, B. Y. Guan and X. W. Lou, *Chem*, 2016, **1**, 102–113.
56 Q. Yang, Y. Liu, M. Yan, Y. Lei and W. Shi, *Chem. Eng. J.*, 2019, **370**, 666–676.
57 Y. Zhang, Z. Li, L. Gong, X. Wang, P. Hu and J. Liu, *J. Energy Chem.*, 2023, **77**, 561–571.
58 D. Chu, F. Li, X. Song, H. Ma, L. Tan, H. Pang, X. Wang, D. Guo and B. Xiao, *J. Colloid Interface Sci.*, 2020, **568**, 130–138.
59 C. Kang, L. Ma, Y. Chen, L. Fu, Q. Hu, C. Zhou and Q. Liu, *Chem. Eng. J.*, 2022, **427**, 131003.
60 M. B. Poudel, A. R. Kim, S. Ramakrishan, N. Logeshwaran, S. K. Ramasamy, H. J. Kim and D. J. Yoo, *Composites, Part B*, 2022, **247**, 110339.
61 Z. Xiao, Y. Mei, S. Yuan, H. Mei, B. Xu, Y. Bao, L. Fan, W. Kang, F. Dai, R. Wang, L. Wang, S. Hu, D. Sun and H.-C. Zhou, *ACS Nano*, 2019, **13**, 7024–7030.
62 F. Zhu, W. Liu, Y. Liu and W. Shi, *Chem. Eng. J.*, 2020, **383**, 123150.
63 P. Du, Y. Dong, C. Liu, W. Wei, D. Liu and P. Liu, *J. Colloid Interface Sci.*, 2018, **518**, 57–68.
64 J. Li, D. Yan, T. Lu, Y. Yao and L. Pan, *Chem. Eng. J.*, 2017, **325**, 14–24.
65 X. Zhou, L. Chen, W. Zhang, J. Wang, Z. Liu, S. Zeng, R. Xu, Y. Wu, S. Ye, Y. Feng, X. Cheng, Z. Peng, X. Li and Y. Yu, *Nano Lett.*, 2019, **19**, 4965–4973.
66 D. Jia, Z. Shen, W. Zhou, Y. Li, J. He, L. Jiang, Y. Wei and X. He, *Chem. Eng. J.*, 2024, **485**, 149820.
67 T. Qiu, S. Gao, Z. Liang, D.-G. Wang, H. Tabassum, R. Zhong and R. Zou, *Angew. Chem., Int. Ed.*, 2021, **60**, 17314–17336.
68 S. Wang, L. Luo, A. Wu, D. Wang, L. Wang, Y. Jiao and C. Tian, *Coord. Chem. Rev.*, 2024, **498**, 215464.
69 E. Doustkhah, R. Hassandoost, A. Khataee, R. Luque and M. H. N. Assadi, *Chem. Soc. Rev.*, 2021, **50**, 2927–2953.
70 B. Li, L. Zhang, Z. Zhao, Y. Zou, B. Chen, X. Fu, F. Wang, S. Long, W. Guo, J. Liang and M. Ye, *Chem. Eng. J.*, 2024, **487**, 150730.
71 Y. Ji, Y. You, G. Xu, X. Yang and Y. Liu, *Chem. Eng. J.*, 2024, **483**, 149365.
72 Y. Ji, W. Li, Y. You and G. Xu, *Chem. Eng. J.*, 2024, **496**, 154009.
73 N. Kitchamsetti and J. S. Cho, *J. Energy Storage*, 2024, **80**, 110293.
74 A. Azhar, M. B. Zakaria, E.-Z. M. Ebeid, T. Chikyow, Y. Bando, A. A. Alshehri, Y. G. Alghamdi, Z.-X. Cai, N. A. Kumar, J. Lin, H. Kim and Y. Yamauchi, *ChemistryOpen*, 2018, **7**, 599–603.
75 K. Li, J. Yang and J. Gu, *Acc. Chem. Res.*, 2022, **55**, 2235–2247.
76 X. Cao, L. Dai, L. Wang, J. Liu and J. Lei, *Mater. Lett.*, 2015, **161**, 682–685.
77 K. Li, Y. Zhao, J. Yang and J. Gu, *Nat. Commun.*, 2022, **13**, 1879.
78 Y. Lu, L. Yu, M. Wu, Y. Wang and X. W. Lou, *Adv. Mater.*, 2018, **30**, 1702875.
79 W. Lu, J. Shen, P. Zhang, Y. Zhong, Y. Hu and X. W. Lou, *Angew. Chem., Int. Ed.*, 2019, **58**, 15441–15447.
80 K. Shi, X. Liu, J. Sang, M. Zhang, D. Han and J. Gong, *Chem. Eng. J.*, 2024, **499**, 156021.

81 K. Wang, M. Yang, Q. Liu, S. Cao, Y. Wang, T. Hu and Z. Peng, *J. Colloid Interface Sci.*, 2025, **678**, 346–358.
82 Y. Huang, Y. Fang, X. F. Lu, D. Luan and X. W. Lou, *Angew. Chem., Int. Ed.*, 2020, **59**, 19914–19918.
83 Y. Li, Y. Zeng, Y. Chen, D. Luan, S. Gao and X. W. Lou, *Angew. Chem., Int. Ed.*, 2022, **61**, e202212680.
84 Y. Fang, X.-Y. Yu and X. W. Lou, *Adv. Mater.*, 2018, **30**, 1706668.
85 H. Xu, Y. Liu, T. Qiang, L. Qin, J. Chen, P. Zhang, Y. Zhang, W. Zhang, W. Tian and Z. Sun, *Energy Storage Mater.*, 2019, **17**, 126–135.
86 J. Lin, C. Zeng, X. Lin, C. Xu and C.-Y. Su, *Adv. Sci.*, 2020, **7**, 2000736.
87 M. Pang, A. J. Cairns, Y. Liu, Y. Belmabkhout, H. C. Zeng and M. Eddaoudi, *J. Am. Chem. Soc.*, 2013, **135**, 10234–10237.
88 Y. Du, J. Gao, L. Zhou, L. Ma, Y. He, X. Zheng, Z. Huang and Y. Jiang, *Adv. Sci.*, 2019, **6**, 1801684.
89 C.-Y. Yang and J.-P. Lang, *EnergyChem*, 2025, 100163.
90 B. Cong, X. Li and G. Chen, *Chem. Eng. J.*, 2023, **460**, 141713.
91 W. Hu, M. Zheng, B. Xu, Y. Wei, W. Zhu, Q. Li and H. Pang, *J. Mater. Chem. A*, 2021, **9**, 3880–3917.
92 G. Wang, A. Gao, T. Zhao, T. Meng, F. Yi, C. Liu, J. Ling, C. He and D. Shu, *Chem. Eng. J.*, 2023, **469**, 143852.
93 H. Hu, J. Zhang, B. Guan and X. W. Lou, *Angew. Chem., Int. Ed.*, 2016, **55**, 9514–9518.
94 Z. Li, L. Zhang, X. Ge, C. Li, S. Dong, C. Wang and L. Yin, *Nano Energy*, 2017, **32**, 494–502.
95 M. Yue, L. Zhong, Y. Sheng, H. He, Y. Xiao, B. Cheng, W. Chen and S. Lei, *Small*, 2024, **20**, 2405262.
96 Q. Li, R. Deng, Y. Chen, J. Gong, P. Wang, Q. Zheng, Y. Huo, F. Xie, X. Wei, C. Yang and D. Lin, *Small*, 2023, **19**, 2303642.
97 Y. Chen, X. Hu, X. Chen, J.-H. Liu, Y. Huang and D. Cao, *Chem. Eng. J.*, 2023, **478**, 147411.
98 X. Wu, C. Yin, M. Zhang, Y. Xie, J. Hu, R. Long, X. Wu and X. Wu, *Chem. Eng. J.*, 2023, **452**, 139573.
99 R. Zhu, Y. Jiang, B. Sun, W. Zhang and H. Pang, *Inorg. Chem. Front.*, 2024, **11**, 8290.
100 Z. Meng, Z. Qiu, Y. Shi, S. Wang, G. Zhang, Y. Pi and H. Pang, *eScience*, 2023, **3**, 100092.
101 X. Liu, M. Yu, J. Liu, S. Wu and J. Gong, *Small*, 2024, **20**, 2306159.
102 J. Łuczak, M. Kroczewska, M. Baluk, J. Sowik, P. Mazierski and A. Zaleska-Medynska, *Adv. Colloid Interface Sci.*, 2023, **314**, 102864.
103 Y. Zheng, S. Zheng, Y. Xu, H. Xue, C. Liu and H. Pang, *Chem. Eng. J.*, 2019, **373**, 1319–1328.
104 H. Zhou, L. Zhang, G. Wang, Y. Zhang, X. Wang, M. Li, F. Fan, Y. Li, T. Wang, X. Zhang and Y. Fu, *ACS Appl. Mater. Interfaces*, 2021, **13**, 39755–39762.
105 C. R. Marshall, E. E. Timmel, S. A. Staudhammer and C. K. Brozek, *Chem. Sci.*, 2020, **11**, 11539–11547.
106 Y. Feng and J. Yao, *Coord. Chem. Rev.*, 2022, **470**, 214699.
107 Q. Chen, M. Yao, Y. Zhou, Y. Sun, G. Zhang and H. Pang, *Coord. Chem. Rev.*, 2024, **517**, 216016.
108 Y. Gan, L. Liu, Q. Zhang, J. Huang, S. Han, B. Chen, Y. Liu, Q. Yu, L. Guan, T. Zhou, M. Han, Y. Zhao and W. Huang, *Energy Storage Mater.*, 2023, **59**, 102794.
109 Z. Li, M. Song, W. Zhu, W. Zhuang, X. Du and L. Tian, *Coord. Chem. Rev.*, 2021, **439**, 213946.
110 X. Zhuang, S. Zhang, Y. Tang, F. Yu, Z. Li and H. Pang, *Coord. Chem. Rev.*, 2023, **490**, 215208.
111 J. Sun, L. Zhang, F. Li, F. Yang, M. Liu, S. Li and D. Zhang, *Adv. Funct. Mater.*, 2025, **35**, 2501181.
112 H. Zou, S. Li, W. Yang, Q. Liu and S. Chen, *Nanoscale*, 2025, **17**, 9480–9489.
113 L. Xing, H. Cheng, Y. Li, Q. Chen and X. Liu, *Chem. Eng. J.*, 2024, **487**, 150729.
114 C. Liu, W. Feng, Y. Bai and H. Pang, *Inorg. Chem. Front.*, 2022, **9**, 5463–5468.
115 H. Ding, Z. Liu, J. Xie, Z. Shen, D. Yu, Y. Chen, Y. Lu, H. Zhou, G. Zhang and H. Pang, *Angew. Chem., Int. Ed.*, 2024, **63**, e202410255.
116 Z. Cui, Q. Li, S. Li, W. Zheng, X. Li, D. Shu, L. Yuan, J. Lu, H. Cheng and T. Meng, *Small*, 2025, **21**, 2410766.
117 Y. Fang, D. Luan, Y. Chen, S. Gao and X. W. Lou, *Angew. Chem., Int. Ed.*, 2020, **59**, 2644–2648.
118 W. Cheng, Z.-P. Wu, D. Luan, S.-Q. Zang and X. W. Lou, *Angew. Chem., Int. Ed.*, 2021, **60**, 26397–26402.
119 Y. Huang, S. L. Zhang, X. F. Lu, Z.-P. Wu, D. Luan and X. W. Lou, *Angew. Chem., Int. Ed.*, 2021, **60**, 11841–11846.
120 Q. Niu, M. Yang, D. Luan, N. W. Li, L. Yu and X. W. Lou, *Angew. Chem., Int. Ed.*, 2022, **61**, e202213049.
121 X. Wang, Y. Chen, Y. Fang, J. Zhang, S. Gao and X. W. Lou, *Angew. Chem., Int. Ed.*, 2019, **58**, 2675–2679.
122 Z. Zhao, J. Ding, R. Zhu and H. Pang, *J. Mater. Chem. A*, 2019, **7**, 15519–15540.
123 R. Zhu, Y. Jiang, Y. Song, L. Liu, Y. Xu and H. Pang, *Chem. Eng. J.*, 2024, **490**, 151681.
124 Z. Sun, Y. Wang, L. Yang, J. Liu, H. Qi, Z. Huang and X. Wang, *ACS Appl. Mater. Interfaces*, 2024, **16**, 584–593.
125 J. Li, X. Qiang, B. Jia, L. Wang and X. Wu, *Appl. Surf. Sci.*, 2025, **695**, 162867.
126 H. Zhang, Z. Li, Z. Hou, H. Mei, Y. Feng, B. Xu and D. Sun, *Chem. Eng. J.*, 2021, **425**, 130602.
127 S. Shi, C. Sun, X. Yin, L. Shen, Q. Shi, K. Zhao, Y. Zhao and J. Zhang, *Adv. Funct. Mater.*, 2020, **30**, 1909283.
128 Z. Zou, Z. Du, L. Dai, D. Liu and W. Du, *J. Am. Chem. Soc.*, 2024, **146**, 31186–31197.
129 D. Wei, B. Ouyang, H. Dong, P. Chen, T. Zhang, B. Wu, Y. He, L. Huang and H. Wang, *J. Energy Chem.*, 2025, **106**, 972–980.
130 Q. Sun, K. Zhu, X. Ji, D. Chen, C. Han, T.-T. Li, Y. Hu, S. Huang and J. Qian, *Sci. China Mater.*, 2022, **65**, 1453–1462.
131 K. Leus, T. Bogaerts, J. De Decker, H. Depauw, K. Hendrickx, H. Vrielinck, V. Van Speybroeck and P. Van Der Voort, *Microporous Mesoporous Mater.*, 2016, **226**, 110–116.
132 D. Bazer-Bachi, L. Assié, V. Lecocq, B. Harbuzaru and V. Falk, *Powder Technol.*, 2014, **255**, 52–59.

133 L. He, Z. Wang, H. Wang and Y. Wu, *Coord. Chem. Rev.*, 2025, **526**, 216361.
134 A. Maiti, R. Biswal, S. Debnath and A. Bhunia, *Energy Adv.*, 2024, **3**, 1238–1264.
135 X.-C. Xie, K.-J. Huang and X. Wu, *J. Mater. Chem. A*, 2018, **6**, 6754–6771.
136 B. Yang, B. Li and Z. Xiang, *Nano Res.*, 2023, **16**, 1338–1361.
137 J. Cai, C. Liu, S. Tao, Z. Cao, Z. Song, X. Xiao, W. Deng, H. Hou and X. Ji, *Coord. Chem. Rev.*, 2023, **479**, 214985.
138 L. Feng, K.-Y. Wang, X.-L. Lv, T.-H. Yan and H.-C. Zhou, *Natl. Sci. Rev.*, 2020, **7**, 1743–1758.
139 X. Liu, M. Yu, S. Wu and J. Gong, *J. Alloys Compd.*, 2023, **969**, 172291.
140 J. Wang, X. Guo, Q. Jing, W. Li, T. Chen, R. Zhu and H. Pang, *Chin. Chem. Lett.*, 2023, **34**, 107675.
141 Z.-T. Pan, Z.-H. He, J.-F. Hou and L.-B. Kong, *Small*, 2023, **19**, 2302788.
142 W.-D. Zhang, Y. Zou, H. Zhao, M. Chen, L. Zhou, X.-R. Xie, X. Yan, H. Pang and Z.-G. Gu, *Small*, 2024, **20**, 2307809.
143 M. Y. Tsang, A. Sinelshchikova, O. Zaremba, F. Schöfbeck, A. D. Balsa, M. R. Reithofer, S. Wuttke and J. M. Chin, *Adv. Funct. Mater.*, 2024, **34**, 2308376.
144 É. A. Santos, L. M. S. Barros, A. F. de F. V. Peluso, I. Galantini, J. M. Gonçalves, R. Maciel Filho and H. Zanin, *Chem. Eng. J.*, 2024, **493**, 152429.
145 Q. Chen, Z. Yang, P. Zhai, W. Luo and Y. Gong, *Adv. Funct. Mater.*, 2025, **35**, 2417923.
146 H. He, L. Wang, M. Al-Abbasi, C. Cao, H. Li, Z. Xu, S. Chen, W. Zhang, R. Li, Y. Lai, Y. Tang and M. Ge, *Energy Environ. Mater.*, 2024, **7**, e12699.
147 A. Fateeva, P. Horcajada, T. Devic, C. Serre, J. Marrot, J.-M. Grenèche, M. Morcrette, J.-M. Tarascon, G. Maurin and G. Férey, *Eur. J. Inorg. Chem.*, 2010, **2010**, 3789–3794.
148 G. Férey, F. Millange, M. Morcrette, C. Serre, M.-L. Doublet, J.-M. Grenèche and J.-M. Tarascon, *Angew. Chem., Int. Ed.*, 2007, **46**, 3259–3263.
149 G. de Combarieu, M. Morcrette, F. Millange, N. Guillou, J. Cabana, C. P. Grey, I. Margiolaki, G. Férey and J.-M. Tarascon, *Chem. Mater.*, 2009, **21**, 1602–1611.
150 D. Asakura, M. Okubo, Y. Mizuno, T. Kudo, H. Zhou, K. Ikedo, T. Mizokawa, A. Okazawa and N. Kojima, *J. Phys. Chem. C*, 2012, **116**, 8364–8369.
151 D. Asakura, C. H. Li, Y. Mizuno, M. Okubo, H. Zhou and D. R. Talham, *J. Am. Chem. Soc.*, 2013, **135**, 2793–2799.
152 X.-J. Wang, F. Krumeich and R. Nesper, *Electrochem. Commun.*, 2013, **34**, 246–249.
153 Z. Zhang, H. Yoshikawa and K. Awaga, *J. Am. Chem. Soc.*, 2014, **136**, 16112–16115.
154 Z. Peng, X. Yi, Z. Liu, J. Shang and D. Wang, *ACS Appl. Mater. Interfaces*, 2016, **8**, 14578–14585.
155 T. Yamada, K. Shiraishi, H. Kitagawa and N. Kimizuka, *Chem. Commun.*, 2017, **53**, 8215–8218.
156 P. Xiong, G. Zeng, L. Zeng and M. Wei, *Dalton Trans.*, 2015, **44**, 16746–16751.
157 S. Maiti, A. Pramanik, U. Manju and S. Mahanty, *Microporous Mesoporous Mater.*, 2016, **226**, 353–359.
158 C. Li, X. Lou, M. Shen, X. Hu, Z. Guo, Y. Wang, B. Hu and Q. Chen, *ACS Appl. Mater. Interfaces*, 2016, **8**, 15352–15360.
159 H. Hu, X. Lou, C. Li, X. Hu, T. Li, Q. Chen, M. Shen and B. Hu, *New J. Chem.*, 2016, **40**, 9746–9752.
160 X. Hu, X. Lou, C. Li, Y. Ning, Y. Liao, Q. Chen, E. S. Mananga, M. Shen and B. Hu, *RSC Adv.*, 2016, **6**, 114483–114490.
161 Z. Xiu, D. Kim, M. H. Alfaruqi, J. Gim, J. Song, S. Kim, P. T. Duong, J. P. Baboo, V. Mathew and J. Kim, *J. Mater. Chem. A*, 2016, **4**, 4706–4710.
162 M. V. Reddy, A. Mauger, C. M. Julien, A. Paolella and K. Zaghib, *Materials*, 2020, **13**, 1884.
163 J. Li, D. Yan, S. Hou, T. Lu, Y. Yao, D. H. C. Chua and L. Pan, *Chem. Eng. J.*, 2018, **335**, 579–589.
164 Y. Shang, H. Li, T. Ma, Y. Yang, Y. Jiang and W. Yu, *ACS Appl. Mater. Interfaces*, 2025, **17**, 31730–31753.
165 N. Huang, H. Zhang, G. Zhu, C. Tang, Z. Cheng, A. Du, M.-S. Wang and H. Zhang, *Chem. Eng. J.*, 2024, **502**, 157959.
166 W. Guo, W. Sun and Y. Wang, *ACS Nano*, 2015, **9**, 11462–11471.
167 S. Chen, L. Shen, P. A. van Aken, J. Maier and Y. Yu, *Adv. Mater.*, 2017, **29**, 1605650.
168 H. Xiao, J. Zhao, Q. Gao, W. Zhang, X. Cheng, C. Song and G. Li, *Chem. Eng. J.*, 2025, **506**, 159927.
169 X. Zhang, H. Xie, Z. Liu, C. Tan, Z. Luo, H. Li, J. Lin, L. Sun, W. Chen, Z. Xu, L. Xie, W. Huang and H. Zhang, *Angew. Chem., Int. Ed.*, 2015, **54**, 3653–3657.
170 R. Gui, H. Jin, Z. Wang and J. Li, *Chem. Soc. Rev.*, 2018, **47**, 6795–6823.
171 C. Ren, Y. Dong and Y. Lei, *Small*, 2025, 2501262.
172 J.-E. Zhou, R. C. K. Reddy, A. Zhong, Y. Li, Q. Huang, X. Lin, J. Qian, C. Yang, I. Manke and R. Chen, *Adv. Mater.*, 2024, **36**, 2312471.
173 H.-J. Liang, X.-T. Li, W.-Z. Zheng, Z.-T. Liu, W. Yang, Z.-L. Liu, Y.-F. Zhang, H.-S. Fan and S.-J. Lu, *Rare Met.*, 2022, **41**, 3381–3390.
174 M. Qi, L. Cheng, X. Zhang, Y. Guo, X. Su, X. Sun, Y. Liu, L. Wang, H.-G. Wang and L. Chen, *Adv. Sci.*, 2025, **12**, 2503369.
175 M. Li, C. Wang, C. Wang, Y. Lyu, J. Wang, S. Xia, J. Mao and Z. Guo, *Adv. Mater.*, 2025, 2416717.
176 Z. Lu, P. Zhang, D. Li, F. Yin, J. Weng and H. Cong, *Chem. Eng. J.*, 2025, **506**, 159896.
177 H. C. Kim, H. Kim, S. O. Moon, C. Jo and H. S. Park, *J. Energy Chem.*, 2025, **105**, 764–796.
178 Y. He, L. Wang, C. Dong, C. Li, X. Ding, Y. Qian and L. Xu, *Energy Storage Mater.*, 2019, **23**, 35–45.
179 J. Xie, X. Li, H. Lai, Z. Zhao, J. Li, W. Zhang, W. Xie, Y. Liu and W. Mai, *Angew. Chem., Int. Ed.*, 2019, **58**, 14740–14747.
180 Y. Zhu, G. Liang, X. Cui, X. Liu, H. Zhong, C. Zhi and Y. Yang, *Energy Environ. Sci.*, 2024, **17**, 369–385.
181 C. Nie, G. Wang, D. Wang, M. Wang, X. Gao, Z. Bai, N. Wang, J. Yang, Z. Xing and S. Dou, *Adv. Energy Mater.*, 2023, **13**, 2300606.
182 B. Fei, Z. Liu, J. Fu, X. Guo, K. Li, C. Zhang, X. Yang, D. Cai, J. Liu and H. Zhan, *Adv. Funct. Mater.*, 2023, **33**, 2215170.

183 H. Raza, S. Bai, J. Cheng, S. Majumder, H. Zhu, Q. Liu, G. Zheng, X. Li and G. Chen, *Electrochem. Energy Rev.*, 2023, **6**, 29.
184 X. Zhang, H. Xie, C.-S. Kim, K. Zaghib, A. Mauger and C. M. Julien, *Mater. Sci. Eng., R*, 2017, **121**, 1–29.
185 Y. Guo, Q. Niu, F. Pei, Q. Wang, Y. Zhang, L. Du, Y. Zhang, Y. Zhang, Y. Zhang, L. Fan, Q. Zhang, L. Yuan and Y. Huang, *Energy Environ. Sci.*, 2024, **17**, 1330–1367.
186 H. Liu, H. Wang, F. Yang, R. Zou, C.-C. Hou and Q. Xu, *J. Mater. Chem. A*, 2025, **13**, 6124–6151.
187 Y. Li, Z. Wang, Q. Zhang, K. Tian, J. Liu, Z. Ni, F. Dong, S. Xiong, X. Lin and J. Feng, *Adv. Energy Mater.*, 2025, **15**, 2406069.
188 Y. Dong, Z. Jin, H. Peng, M. Wang, S. Ma, X. Li, Y. Ren, L. Xie and J. Zhang, *Small*, 2025, **21**, 2412186.
189 Y. Wang, R. Niu, L. Chen, Y. Yang, H. Yu and X. Qiu, *Chem. Eng. J.*, 2025, **512**, 162305.
190 M. Gao, F. Wang, S. Yang, A. Gaetano Ricciardulli, F. Yu, J. Li, J. Sun, R. Wang, Y. Huang, P. Zhang and X. Lu, *Mater. Today*, 2024, **72**, 318–358.
191 B. Ji, W. Li, F. Zhang, P. Geng and C. M. Li, *Small*, 2025, **21**, 2409273.
192 U. A. Kolachi, N. H. Solangi, Y. Sun, R. Andavar, I. Shahid, J. Zhao and J. Pan, *J. Mater. Chem. A*, 2025, **13**, 22142–22154.
193 J. Wang, S. Li, N. Fu, D. Tian, Y. Zheng, F. Wang, C. Liu, X. Wang, Z. Zhou, Y. Niu, H. Liu, G. Wang, S. Mu and J. Luo, *Adv. Compos. Hybrid Mater.*, 2025, **8**, 190.
194 Y. Xie, X. Gao, H. Wang, C. G. Nuñez, F. Jiang, Q. Li, H. Bai, F. Yao and H. Yue, *Chem. Eng. J.*, 2025, **518**, 164964.

